DENDRONIC SURFACES FOR DETECTION OF EXPLOSIVE VAPORS

by

Ja'be G. Kiri

A Thesis Submitted in Fulfillment
of the Requirements for the Degree of
Master of Science

Middle Tennessee State University
December 2013

Thesis Committee:

Dr. Andrienne C. Friedli, Major Professor

Dr. Dwight J. Patterson, Reader

Dr. Charles C. Chusuei, Reader

ACKNOWLEDGEMENTS

I would like to give thanks to my friends Angela Johnson, Jenae Matikke and Kaitlen Howell for helping me with my son so that I could continue with school. They are such great friends to me and I will forever be grateful to them. I would also like to thank my committee members Drs. D. Patterson and C. Chusuei for taking time out of their busy schedules to read my thesis and help me with corrections. Furthermore, I would like to give thanks to the Chemistry Department faculty and staff, especially Mandy Burns for weekly comic relief and Mr. Jessie Weatherly for his constant help with the instruments. Last but not least, I would like to thank my advisor Dr. Andrienne Friedli for guiding me throughout my project. She has been more than just a major professor to me. I am more than happy to have her in my life throughout college.

ABSTRACT

International terrorism, homeland security, and the remains of landmines throughout the world have increased interest in the detection of explosive materials. Non-contact methods for sensing explosives in the field are necessary worldwide. 2, 4-Dinitrotoluene (DNT) is model for 2, 4, 6-trinitrotoluene (TNT), a readily-available explosive. The focus of this project is to make a sensor based on dendrons (tree-like polymers on surfaces) that can detect DNT. In the work described here, a modification of the literature synthesis of melamine dendrons that was synthesized and characterized by Simanek, Shantz and coworkers was used. The sensor design included a high surface area substrate made of mesoporous silicate (m-SiO_2) films and solids. The dendrons were built on the substrates via an iterative method and a phenol added through an imine linkage (**Figure 1**). Calculations indicated that G1-imine dendrons should have greater affinity for DNT than G1 alone based on H-bonding interactions of the DNT nitro group oxygens with the phenol proton.

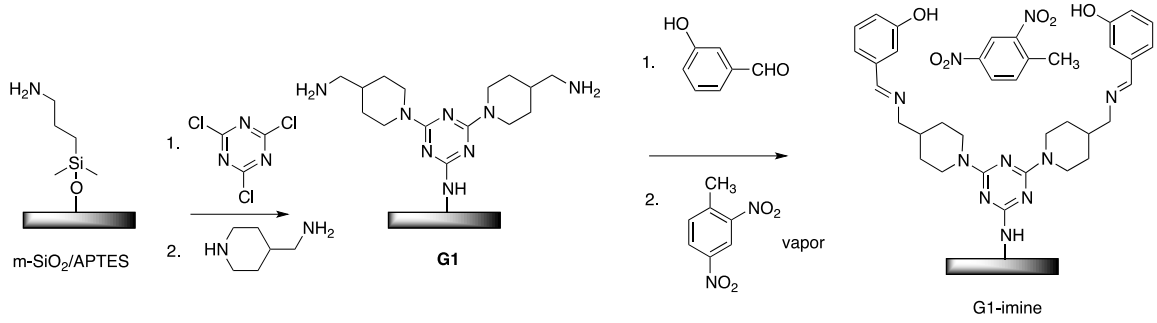

Figure 1. Imine formation from surface-bound G1 and proposed interaction with DNT vapor.

The solid dendronic materials were analyzed using thermogravimetric analysis (TGA) and Fourier Transform Infrared Spectroscopy (FTIR) before and after exposure to DNT. Films were characterized by Ultraviolet Spectroscopy (UV).

TABLE OF CONTENTS

PAGE

LIST OF FIGURES

FIGURE **PAGE**

LIST OF TABLES

TABLE **PAGE**

CHAPTER 1

INTRODUCTION

Mesoporous silicates have been studied for decades,[1] and have proven to be very useful in a variety of applications including pre-concentrators,[2] chemical sensing probes,[3] molecular filters,[4] energy transfer devices, catalysts, microelectronic low dielectric constant films, and selective sensors.[5] A common sensor application is biosensors, a subset of sensors that are highly desired in disease diagnosis and drug discovery.[6] Another common sensor application is explosives detection, due to the current era of heighted risk for terrorism within the US. Common explosives are shown in Figure 1: cyclotrimethylene trinitramine, RDX (Research Department eXplosive or Royal Demolition eXplosive)[7] and 1,2,3-trinitroxypropane (NG).[8] The compound 2,4-Dinitrotoluene (DNT) was chosen as a model for TNT in this study because the structures are closely related, but DNT is not explosive and less regulated than TNT.[9] DNT is a pale yellow crystalline solid that is a precursor to 2,4,6- trinitrotoluene (TNT)[9] and it is mainly used in the polymer industry as a plasticizer.[10]

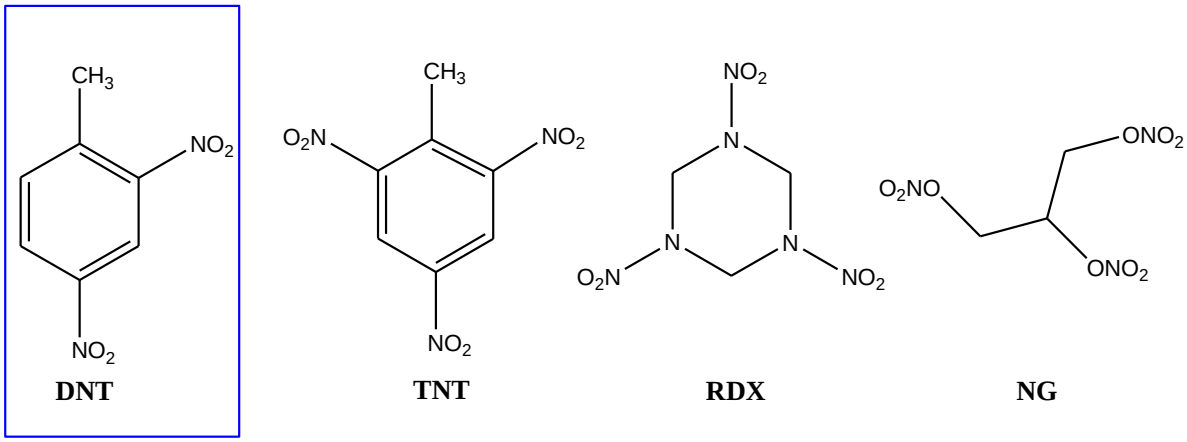

Figure 1. Structures and abbreviations for common explosives.

Mesoporous silicates (m-SiO_2) are good substrates for sensors because they are capable of providing advantages such as accessibility to functionality,[11] mechanical stability,[6] chemical inertness,[12] and high surface area,[12] stability over a wide range of pH (excluding alkaline pH values), relative and transparency in the UV-visible spectrum.[13] The prefix "meso-" refers to a region 2 to 50 nm, "macro-" to a region > 50 nm, and "micro-" to a region < 2 nm.[13]

Mesoporous silicates are derived from sol-gel synthesis (a wet chemistry technique used for making glasses and ceramics). This technique involves preparing a solution (sol) that becomes a glass (gel) once dried. Figure 2 illustrates the structure in m-SiO_2 with hexagonal pores.

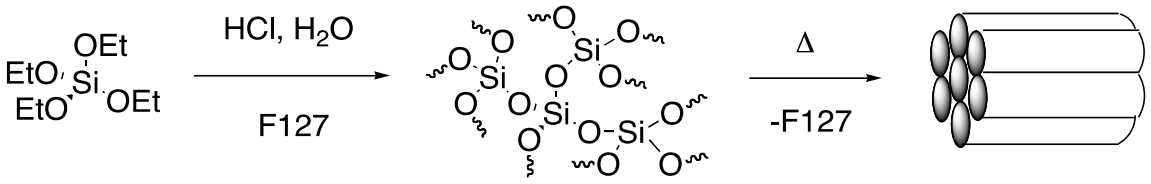

Figure 2. Chemical equation showing the formation of pores in m-SiO_2.

There are several ways for making hybrid inorganic-organic mesoporous silicates. Silanol groups at the surfaces of mesoporous silicates can be grafted with organosilanes such as 3-aminopropyl trimethoxysilane (APTMS), 3-mercaptopropyltrimethoxysilane (MPTMS) and hexamethyldisilazane (HMDS).[2] Pores that are larger compared to the size of the group to be incorporated are used to avoid pore blockage and to achieve a uniform distribution of functional groups at the surface.[13] The synthesis of mesoporous silica is accomplished by carrying out sol-gel chemistry in the presence of micelles[14] (Figure 3). Micelles are an aggregation of surfactant molecules dispersed in a solvent containing colloids, substance microscopically dispersed evenly throughout another substance, [15] as shown in Figure 4.

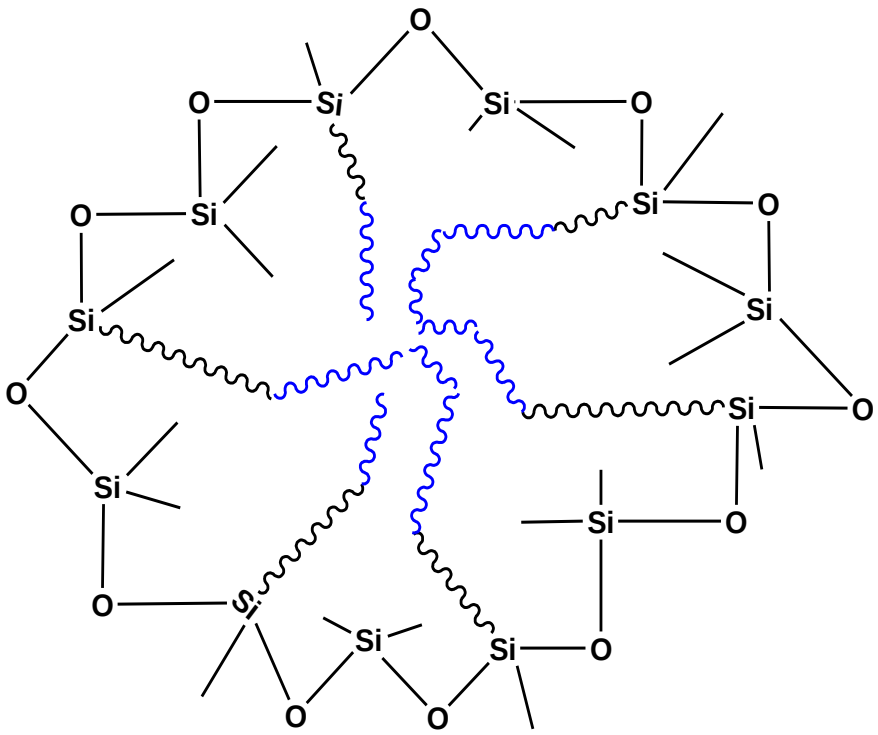

Figure 3. Structure of micelle made hexagonal silica/block copolymer m-SiO_2 with the polypropylene oxide/poly(ethylene oxide)/silica separated.[14]

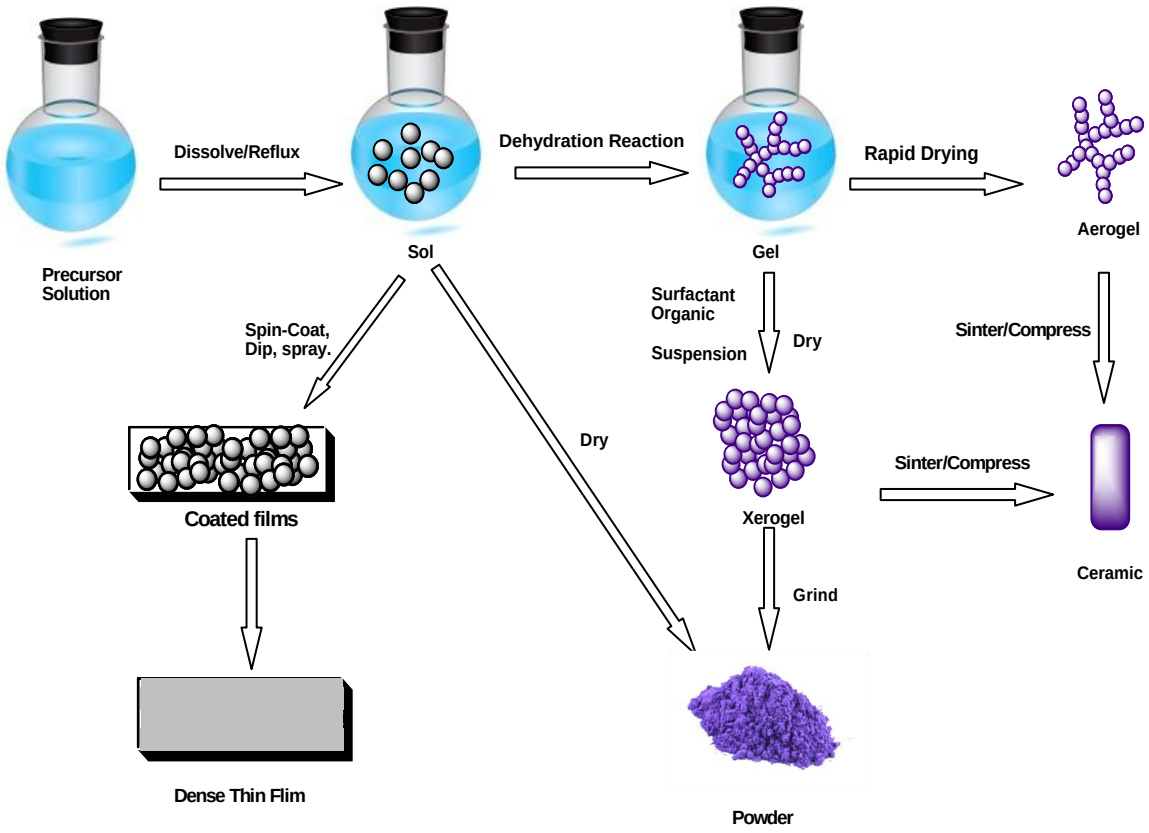

Figure 4. Overview of sol-gel procedure showing the differences between xerogels and aerogels.[13]

The most commonly-used sol-gel precursors are tetraethoxysilane (TEOS) and tetramethoxysilane (TMOS).[13] Drying a gel under ambient conditions, or with heat, will usually cause the gel to shrink as the solvents leave the micropores of the silicate network resulting in xerogel.[2] However, controlling the drying can remove the solvent in such a way as to yield a product that is similar to the size and the shape of the original gel (aerogels).[13] Organic pore templating materials can be added during the sol phase,

become entrapped in the gel, and then be removed by calcification (baking) or extraction with solvent. This result in a large effective surface area pore volumes and controllable pore sizes.[15]

Several mesoporous materials with different structures have been synthesized and grouped into families based on their synthesis approach. For example, mesoporous silica (M41S) materials are synthesized by employing catonic alkylammonium surfactants in amounts above their critical micelle concentrations.[13]

The pore size of mesoporous polymer/silica hybrid could be controlled using different types and concentrations of surfactant. Mesoporous materials can have hexagonal (called mesocellular materials (MCM)),[5] fused silica material (FSM) which are also hexagonal,[16] spherical bicontinuous (SBA),[5] cubic (3D),[11] or wormlike (disorganized). We will be focusing on hexagonal pores.[17]

Ever since the report of a surfactant-templated m-SiO_2, a variety of ionic and non-ionic surfactants, and a combination of both have been studied. Ordered surfactant materials have been synthesized using surfactants with concentrations that are above their critical micelle materials where inorganic-organic self-assembly occurs.[14] Surfactants are removed by calcination /burning to produce molecular sieves with narrow pore size distributions and highly ordered mesostructures.[13] MCM-48, which has three dimensional cubic order, MCM-41, which has a two-dimensional hexagonal alignment of mesopore channels, and MCM-50, which functions as a layered material, are all part of the M41S

family.[13] Fused silica materials (FSM-16) are mesoporous silicates with hexagonal order and are formed by an inorganic-nonorganic self-assembly process.[13]

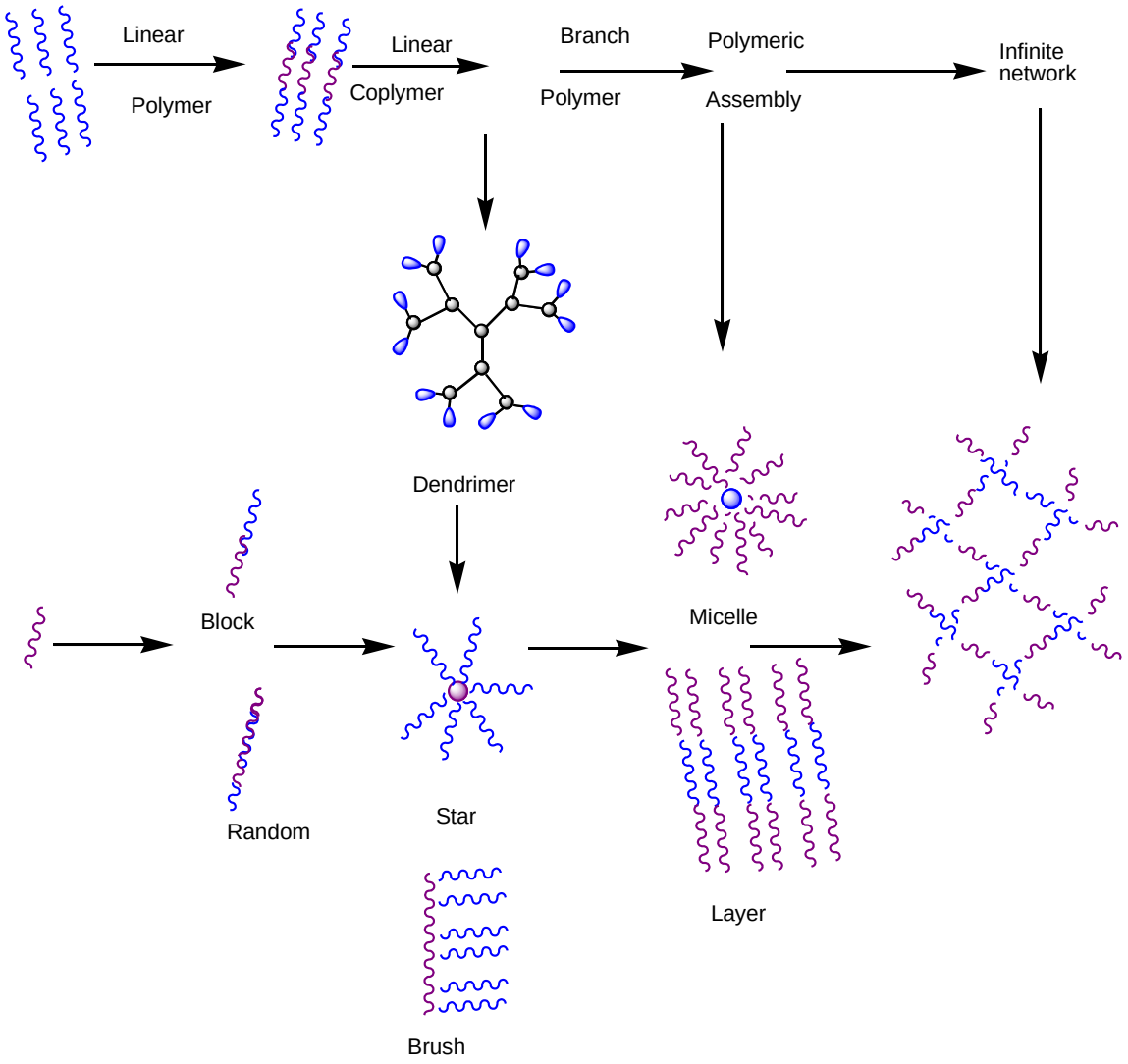

Figure 5. The progression between linear and networked polymers.[18]

Alkyamines have been used as surfactant to prepare several mesoporous molecular sieves (MSUX) with pore sizes from 1.5 to 10 nm. Series with wormlike mesopores were templated with poly (ethylene oxide) surfactants.[19] Block copolymers have generated the SBA family of materials.[20, 21] The SBA-15 silicate has a well-ordered hexagonal mesoporous structure[22] analogous to MCM-41, often with micropores that allow interconnectivity between pore channels.[13]

In this work we used the non-ionic surfactant triblock-copolymer Pluronic F-127[23] [poly(ethyleneoxide)-block-poly(propyleneoxide)-block-poly(ethyleneoxide), $(PEO)_{106}(PPO)_{70}(PEO)_{106}$, a triblock copolymer of polyethylene oxide (PEO) and polypropylene oxide (PPO)[23] that terminates in a primary hydroxyl. This was chosen because it is a well-characterized material that has been used to create porous materials for optical sensors.[5]

Due to the need to detect explosives such as those in Figure 1, sensors for DNT based on fluorescent and electrochemical detection have been reported. One of the first DNT sensors was based on quenching of fluorescent conducting polymer upon exposure to DNT vapor.[24] (Mesoporous SiO_2 sensors for nitroaromatics, include a fluorescent sensor using silanes (pyrene, fluorescein, dansyl) to detect the presence of nitroaromatics, including DNT, at pressures as low as 1.4 ppm through fluoresence quenching.[25] Vu, *et. al* [26] also reported a sensor based on fluorescence quenching using m-SiO_2 with wormlike, hexagonal, and cubic morphologies and different modes of attachment of

pyrene fluorophores.[27] Another fluorescent sensor used porphyrin and metallo-porphyrin-doped silica films to demonstrate that fluorescence quenching with nitroaromatics is affected by pore structure [28,29] Amine-coated m-SiO_2 microspheres on glassy carbon electrodes gave high reduction peak currents for nitroaromatic compounds due to the strong interaction between the electron deficient nitro N atoms and the electron-rich amine N atoms. [30] Surfactant/m-SiO_2 layers detected linear current responses to nitroaromatics in solutions down to nanomolar concentrations .[31]

The sensing material of interest in this research is dendrimers (Figure 6).[32] A dendrimer is a highly polybranched, nonlinear and polyfunctionalized tree-like polymer [27] with a well-defined structure, uniform size and molecular weight.[33-37] Unlike linear polymers, they have perfectly defined structure and molecular weight, due to their interactive step-by-step synthesis [27] (Figure 7).[38] Dendrimers can form stable, dense, well-organized, and close-packed arrays on substrate surfaces,[39] have multiple branched ends,[40] and multifunctional ends.[41]

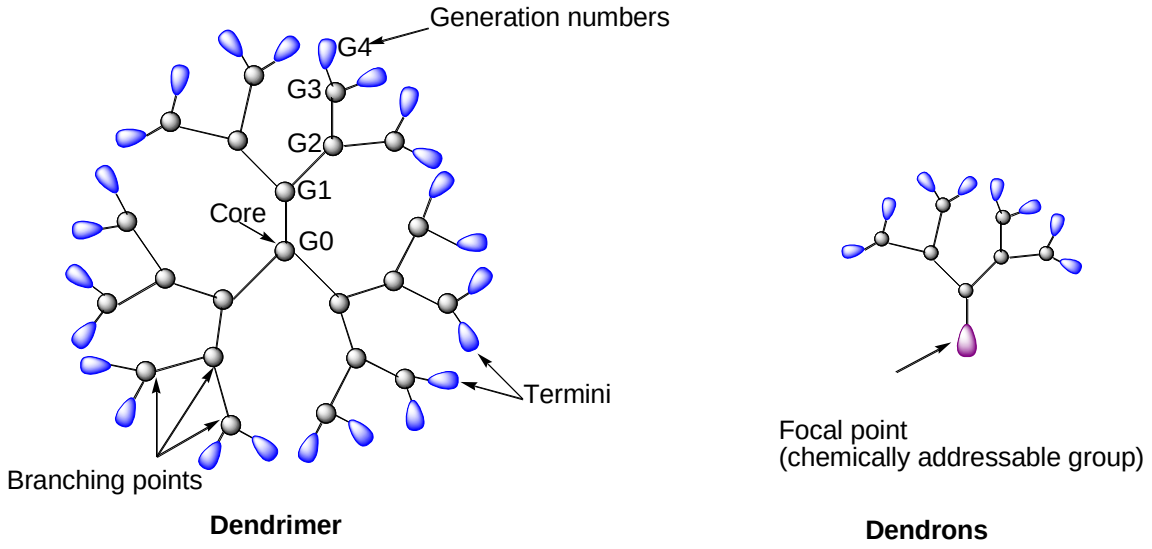

Figure 6. Schematic of the structure of dendrimers and dendrons, where the focal point is the surface.[32]

There are two types of dendrimers as defined by their shapes. The first one has a circular or elliptical shape in which repeat units regularly repeat from a core,[42, 43] and the second one has a conical shape with repeat units directionally built from a core.[44-46] Numerous applications for dendrimers molecules have been found in different fields such as catalysis,[47-50] biomedicine[51], energy or charge-transfer systems,[51-55] sensors,[56]and charge transfer of light-emitting layer in organic light emitting diodes (OLEDs).[57,58] These applications succeed due to some specific advantages of dendrimers: the size and structure are controllable and at the same time it is possible to introduce different kinds of functional groups into their terminal groups/cores. Above all, dendrimers have shown evidence of a highly-ordered structure and produce thin films with various functional

groups on the top surface of the substrate. This allows control of surface properties at the molecular level.[59] This is especially relevant to us because our goal is to make thin film vapor sensors using dendrimers.

There are three distinguishable structural characteristics of dendrimers, namely a central core unit, one or more series of radial branches, and functional groups affixed on the outermost series of branches.[15] Dendrimers are built from either a divergent route (initiating from the core unit) or from a convergent route (initiating from the functional groups) [60](Figure 7). In the divergent methods, dendrimers grows outwards from a multifunctional core molecule. The core unit is like a hub from which the radial growth of the dendrimers originates. The core molecule reacts with the monomer molecule containing one reactive and two dormant groups giving the first generation dendrimers.[61] After the first series of branches are added onto the core, a point of divergence is created at the end of each branch. This point of divergence will enable

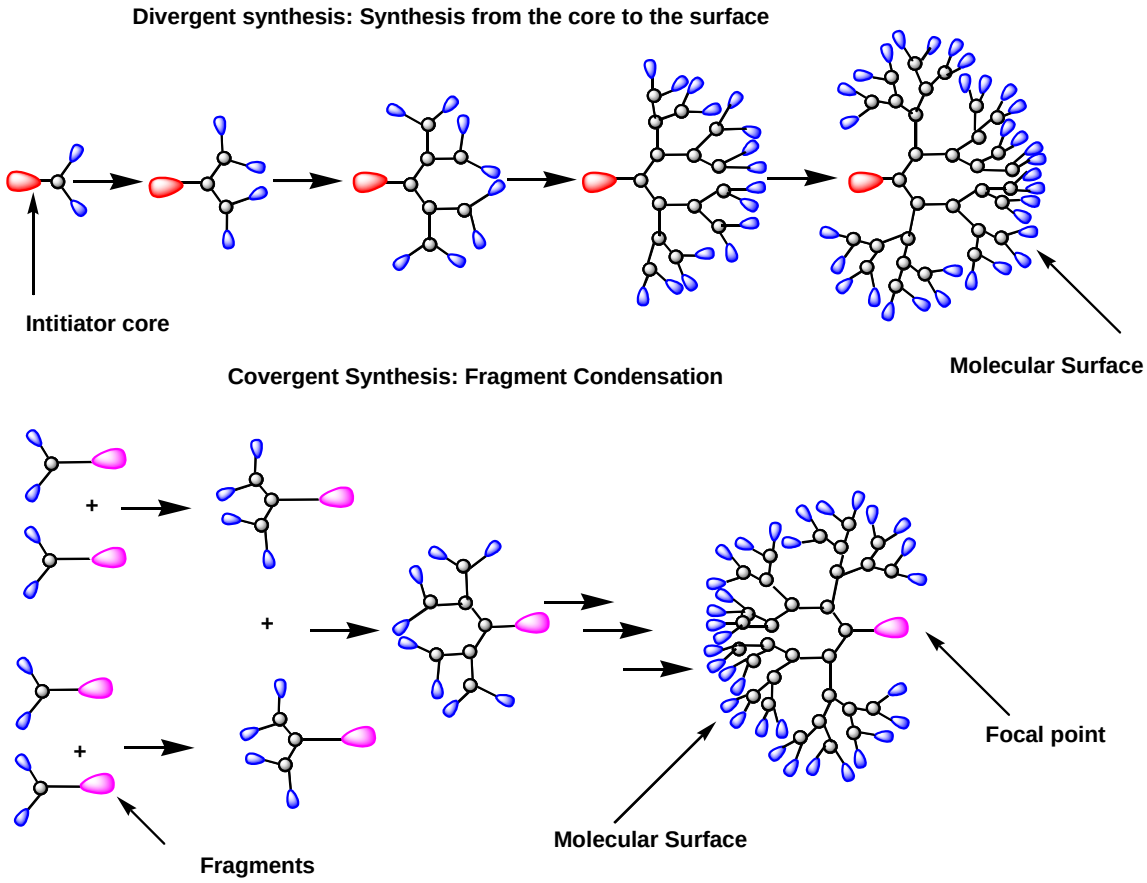

Figure 7. The differences in the divergent and convergent synthesis of dendrons[38]

dendritic growth at the next step of the synthesis. As each generation is being built, and added onto the core, the number of repeating units determines the generation of the dendrimers.[15] Several generations of surface dendrimers are built layer after layer. The divergent synthesis of dendrimers ends when functional groups are grafted at the points of divergence in the last generation of branches.[15] In the convergent approach, the

dendrimers are constructed in a stepwise manner starting from the end groups and progressing inwards.[61] When the growing branched polymeric arms (dendrons) are large enough as needed, they are attached on to the multifunctional core molecule. The resulting flexibility in molding dendrimers architecture has the advantage that they can be used as core units to prepare desired materials.[62] Hydrolysis and condensation of the dendrimers periphery-grafted silicon-alkoxy groups and the subsequent removal of the templates carry out the synthesis of these networks by calcification.[62]

Aromatic dendrimers can be synthesized from several different amines. For example, Czerniewski *et al* [62] have synthesized silica based network using 3,5-dihydroxybenzylamine (DHBA)-based dendrimers as templates and have demonstrated the role of dendrimer aggregation and the type of silane reagent employed in the reaction, on the evolution of the network structure. Morales-Espinoza *et al*[59] reported the synthesis of two generations of dendrimers with molecules of pyrene on the periphery and a tetraphenylporphyrin core by applying the convergent pathway. Lastly, Yoo *et al* reported the synthesis and characterization of melamine-based dendrimers / SBA-15 hybrids.[63]

Dendrimers and dendrons have been used as sensors for organic molecules previously. Dendrimers[64] and surface-bound dendrons [65] were previously observed spectroscopically to entrap guest molecules including dyes and organic solvents, respectively. Absorption of CO_2 into dendron-modified solid m-SiO_2 was quantified

using thermogravimetric analysis.[66] The maximum CO_2 capacity for melamine-based dendronic -G3 solid was 4%,[67] comparable to that of PAMAM-G3,[68] but lower than the 7-8% reported for related TREN-G3 dendrimer.[66]

Here, we report the synthesis and characterization of dendrons built on m-SiO_2 films through a modification of the method of Schantz and Simanek[63] on films and solid surfaces and modifying the dendron surface through an imine linkage to make a sensor for 2,4-DNT.

The sensing device ultimately will be a Bloch wave sensor composed of a multilayered substrate made of alternating layers of SiO_2 and TiO_2.[69] Upon irradiation with an appropriate wavelength laser, this photonic band gap material (PBG) generates an evanescent wave that travels inside the last layer of the material and in the air interface above it. At a certain angle of incidence, the surface wave disappears, and this angle of this mode depends upon the amount and nature of material at the interface and in the last layer of the PBG material. No active label is needed for the sensor, just independent spectroscopic confirmation that the analyte of interest is present. The utility of this sensor has been confirmed for protein/antibody recognition.[70] Detection of vapors and spores under flow cell conditions are still under investigation.[71]

CHAPTER 2

EXPERIMENTAL

2.1. MATERIALS

3-(Aminopropyl)triethoxysilane (APTES, 99%), tetraethoxysilane (TEOS, ≥99%) and 2,4-dinitrotoluene (DNT), were purchased from Sigma-Aldrich (Milwaukee, WI). Hydrochloric acid (HCI) ethyl acetate, hexanes, and ethanol (EtOH) were purchased from Fisher Scientific (Pittsburg, PA). Anhydrous toluene, methanol (MeOH), chloroform ($CHCl_3$), dichloromethane (CH_2Cl_2) and tetrahydrofuran (THF), (all ACS reagent grade) and Pluronic F-127 $(PEO)_{106}(PPO)_{70}(PEO)_{106}$, *N*,*N*-diisopropylethylamine (DIPEA, 99%), cyanuric chloride (99%), tetramethylsilane (TMS), and 3-hydroxybenzaldehyde were also purchased from Sigma-Aldrich (Milwaukee, WI). 4-(Aminomethyl)piperidine (AMP, ≥98%) was purchased from TCI. All chemicals were used as received.

2.2. PREPARATION OF MESOPOROUS MATERIAL

2.2.1. Substrate Cleaning

Fused silica slides (1" x 1", Dell Optics) and silicon wafers 2 inch wafers cut into quarters, (Wafer World) were cleaned by rinsing them with methanol. Nitrogen gas ($N_{2)}$ was used to thoroughly dry the slides.

2.2.2. Sol-gel Preparation and Film Formation

The sol-gel was synthesized according to Wirnsberger[21] by adding EtOH (13 mL, 222.65 mmol), to F-127 (2.00 g, 0.158 mmol), then TEOS (4.55 mL, 20.4 mmol), H_2O (0.80 mL, 44.4 mmol), and 2 M HCl (0.112 mL, 3.65 mmol) in a round bottom flask. The solution was heated at reflux for 1 h and cooled at room temperature before spin-coating onto Si wafers. (Aliquots of 40 μL were spin coated on fused silica or silicon wafers at 2000 rpm for 30 s. The films were kept in a desiccator containing water for 24 h to prevent cracks and stored in a laminar flow hood to avoid dust.

2.2.3. Calcination of Films and Solids

After the films and the wafers were coated with the sol-gel solution, the remaining sol-gel was dried at 80 - 100 °C. Partially-dried films on silicon or glass substrates, and evaporated solid samples (10 - 20 mg) were calcined by placing them in ceramic boats, which were then heated at 1°C/min to 400 °C, then 1°C / min to 600 °C in a programmable Lindberg quartz tube furnace for 4 h because thermogravimetric analysis (TGA- see below) indicated that the F-127 was completely removed by 700 °C**.** The calcification process was carried out in air.

2.2.4. Treatment with APTES: Films

After calcification, the films and solids were treated with solutions of 3-aminopropyl triethoxysilane. Three different concentrations were used. A concentration of APTES solution was prepared from APTES 230 µL (0.218 g, and 0.983 mmol) and 100 mL of anhydrous toluene in a clean and dry volumetric flask in a dry box. Each APTES solution was poured into a staining jar containing films on silicon wafers and was immersed for 1 h. Additionally a 1% w/w solution of APTES 500 µL (0.473 g, 1.96 mmol) was prepared in 100 mL toluene and left immersed overnight. A 1% w/w solution of APTES 500 µL (0.473 g, 1.96 mmol) was referred to as the high concentration APTES and the other as the lower concentration APTES 230 µL (0.218 g, 0.983 mmol). The coated films were each rinsed in toluene twice, dried under a stream of nitrogen gas and heated on a hotplate for 10 min at 110 °C to remove the toluene and complete the polymerization of the silane coating.

2.2.5. Treatment with APTES: Solids

To coat the solids with APTES, the concentrations were scaled up by 5 times and 5.0 g solid m-SiO_2 was used. The lower concentration APTES 800 µL (0.759 g, 3.42 mmol, 0.68 mmol/g) in 100 mL of anhydrous toluene and higher concentration of APTES 1.15 mL (1.09 g, 4.91 mmol) in 100 mL toluene were each prepared in a volumetric flask. 5.0 g batch of m-SiO_2 was placed into a 200 mL round bottom flask with APTES

solution and was immersed for 1 h. Additionally a 0.5% w/w solution of APTES 500 µL (0.473 g, 2.1 mmol) was prepared in 50 mL toluene and 1.0 g m-SiO_2 solid left immersed overnight. The solids were filtered on fritted glass funnel, then rinsed with toluene (100 mL), filtered, and air dried overnight.

2.3. PREPARATION OF DENDRONS

2.3.1. Melamine Dendrons

The synthesis of melamine dendrons was performed according to a procedure from the literature.[63] Synthesis of one generation was accomplished by combining amine-functionalized m-SiO_2 (0.50 g) with cyanuric chloride (CC) solution (12.5 mL 0.3M), which is prepared from CC (1.25 g, 6.78 mmol) and diisopropylethylamine (DIPEA) (1.86 g, 14.35 mmol) in tetrahydrofuran (THF, 25 mL). The test tube was shaken using a thermal rocker (Model No. 463, Thermo Scientific) for approximately 24 h at 40 °C ± 2 °C. The solution was filtered using fritted glass funnel to remove the m-SiO_2 from the solution, and the silica was then rinsed with 25 mL portions each of methanol, dichloromethane and THF sequentially. The silica was transferred back into a clean test tube, and a 12.5 mL of a 0.4 M 4-(aminomethyl)piperidine (AMP) solution added. This was prepared by adding AMP (1.25 g, 10.96 mmol) to THF (25 mL). The test tube was again shaken for 24 h at 40 °C ± 2 °C. The solid material was filtered and rinsed as

described previously to give 0.48 g (G1). The same procedure was followed to increase the dendron generations from G1 to G2 (~0.47 g) and G3 (~0.46 g).

2.3.2. Imine Model Compound

A solution of 4-(aminomethyl)piperidine (AMP, 228 mg, 2.0 mmol) and 3-hydroxybenzaldehyde (244 mg, 2.0 mmol) were placed in round-bottomed flask containing THF (10 mL). The solution was heated at reflux for 2 h or until complete. NMR showed that the reaction was >90% complete after 1 h. The solvent was removed under reduced pressure to give a pale yellow glassy product (401 g, 96%). This complex with THF was recrystallized from ethyl acetate and hexanes to give a waxy off white solid. ^{1}H NMR ($CDCl_3$) δ 1.20-1.28 (m, 2H), 1.75 (d, J=12.6 Hz, 2H), 1.80-1.88 (m, 1H), 2.65 (dt, J=12.6, J=2.3 Hz, 2H), 3.15 (d, J=12.6 Hz, 2H), 3.47 (d, J=6.3 Hz, 2H), 5.61 (bs, 2H), 6.88 (dd, J=8.1, 1.8 Hz, 1H), 7.08 (d, J=7.5 Hz, 1H), 7.23 (t, J=7.7 Hz, 1H), 7.27 (d, J=4.4 Hz, 1H), 8.15 (s, 1H); ^{13}C NMR δ: 30.91, 37.17, 45.73, 67.18, 113.63, 118.92, 120.35, 129.79, 137.17, 157.97, 161.86. IR: 3051 cm^{-1}, 2922 cm^{-1}, 2843 cm^{-1} , 1644 cm^{-1}, 1583 cm^{-1}, 1454 cm^{-1},1273.66 cm^{-1}.

2.3.3. Synthesis of Imine Dendrons on m-SiO_2 Solids

The synthesis of the imine derivative was carried out by suspending m-SiO_2-G1 (0.313 g) in THF (5 mL) and adding 3-hydroxybenzaldehyde (12 mg, 0.10 mmol). The

solution was heated at reflux for 1 h. The solid was filtered and rinsed with EtOH (50 mL) and air dried. For the G2 the amount of 3-hydroxybenzaldehyde was doubled (24 mg) and for G3 it was tripled (36 mg) to allow sufficient excess for the each generation. Ethanol was used originally as solvent, but appeared to remove the dendrons from the substrate. Another imine derivative was carried out for the G1 with high concentration of APTES. The same procedure was conduct using m-SiO_2 (0.200 g) in THF (5 mL) and adding 3-hydroxybenzaldehyde (122 mg, 1.00 mmol). The solution was heated at reflux for 8 h.

2.3.4. Synthesis of Imine Dendrons on m-SiO_2 Films

The synthesis of the imine derivative on films was carried out by dissolving 3-hydroxybenzaldehyde (12 mg, 0.10 mmol) and in THF (5 mL) in a Teflon jar with a screw cap lid. The sample was rocked using a thermal rocker for at 40 °C for 1 h.
To allow sufficient excess for the each generation, the amount of 3-hydroxybenzaldehyde was doubled (24 mg for G2) and tripled (36 mg for G3). Ethanol was used originally as solvent, but appeared to remove the dendrons from the substrate.

2.4. Imine Characterization

2.4.1. Thin Layer Chromatography (TLC) and Nuclear Magnetic Resonance (NMR)

To analyze the progress of the imine reaction, thin-layer chromatography (TLC) was conducted using 50% ethyl acetate in hexanes. The solvent was evaporated using a rotary evaporator (Buchi- RII). TLC was performed on glass plates coated with silica gel and UV active backing (silica gel, 60 Å 230-400 mesh ASTM) purchased from Fisher Scientific, Pittsburg, PA. The TLC plates were analyzed with short wavelength (254 nm) UV light. Nuclear Magnetic Resonance (NMR) was conducted to check for structural composition of the compounds. The NMR data was obtained by using an ECA-500 JEOL 500 MHz NMR. Deuterated chloroform ($CDCl_3$) was the solvent used to perform the NMR. Chemical shifts are reported in parts per million using tetramethylsilane (TMS) as an internal reference. Splitting patterns are designated by the following: s (singlet), d (doublet), t (triplet), q (quartet), app t (apparent triplets), app q (apparent quartet), m (multiplet), and dd (doublet of doublets). The coupling constants (J values) are recorded in Hertz (Hz). Chemical shifts are assigned to NMR spectra based on ^{1}H (proton), ^{13}C (Carbon).

2.4.2. Calculated Equilibrium Geometries

Equilibrium geometries were calculated using AMI program in the Spartan '04 (Wavefunction) graphic interface program. The equilibrium geometry was calculated

using Hartree Fock 3-21G* basis set, followed by 6-31G**. The keyword MAXCYCLE=300 was used to allow minimization to complete. The shortest hydrogen bonding distances between primary amine hydrogens nearest each nitro group oxygen in DNT were determined. For intermolecular interactions in which the DNT formed a pi complex with the triazine ring in the dendron, shortest distances between triazine N and DNT nitro N distances were determined.

2.5. SAMPLE ANALYSIS

2.5.1. Thermogravimetric Analysis (TGA)

Thermogravimetric analysis (TGA) is a technique that is used to determine the amount and rate of change in the weight of a material as a function of temperature/time in a controlled atmosphere. Because TGA uses heat to induce reactions and physical changes in the samples being analyzed, these measurements are used to determine the composition of materials and to predict their thermal and/or oxidative stability, and decomposition kinetics at temperatures up to 1000 °C. Samples that can be analyzed by TGA include polymers, hybrid materials, foods, fine chemicals, explosives, and industrial samples. Quantitative measurements of a sample's characteristic mass change from dehydration, decomposition, and oxidation of a sample are correlated with heating rates and temperature ranges. It can also provide information about the composition of multicomponent systems, an estimate of the lifetime of a product, the moisture and

volatiles contents of materials, and the effect of reactive or corrosive atmospheres on the material.

2.5.2 Solid Characterization with TGA

Thermogravimetric Analysis (TGA) was conducted on a TA Instruments Q-500. After initial taring of empty platinum TGA pans, solid samples (10 - 20 mg) were placed on the pans and heated from 25 - 600 °C at a rate of 10 °C/ min under nitrogen. Flow rates to the furnace (sample) were between 38.0 and 40.0 mL / min, while flow rates to the balance ranged from 22.5 to 25.6 mL / min. The amount and rate of change in the weight of each sample were recorded as a function of temperature. A control experiment determined the temperature program used to remove F-127 slowly from the m-SiO_2. After initial taring of empty platinum TGA pans, the template polymer F-127 (10 - 20 mg) was placed on the pan and heated from 25 - 800 °C at a rate of 10 °C / min under nitrogen gas. The result is shown in Figure 8. Also a TGA was run on m-SiO_2 powder as a control and showed no appreciable weight loss other than water.

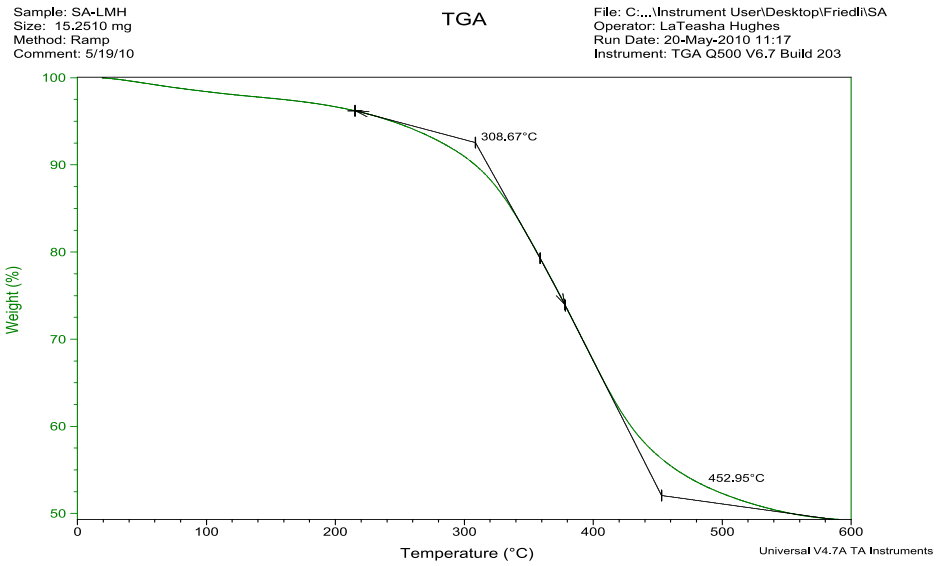

Figure 8. TGA of solid m-SiO_2 prepared with F-127.

To determine the weight percentage attributed to each generation (G1, G2, and G3) of dendrons, TGA was run on solid samples. Several consistent weight losses event were identified and assigned as arbitrary ranges for purposes of comparison. Base on the boiling temperature of the samples,the first range was 25 - 130 °C and was assigned to loss of solvents trapped in the samples. The second weight loss was observed between 130 °C and 200 °C and assigned to C-C bond breakage. A third weight loss occurred between 400 °C and 800 °C and was attributed to burn-off of residual aromatic groups.

2.5.3. Fourier Transform Infrared Spectroscopy (FTIR)

IR radiation refers to the broad part of electromagnetic spectrum that is between the visible and microwave region. The IR radiation frequencies of 10,000 - 100 cm^{-1} are absorbed and converted by molecules into energy of molecular vibration. IR is a helpful technique for identification of organic compounds due to characteristic functional group absorptions between 400 cm^{-1} and 4000 cm^{-1}. In addition, it only requires a very small amount of sample for analysis and even simple molecules can give an extremely complex spectrum. IR can identify unknown materials, the quality or consistency of a sample, and also quantify the amount of components in a mixture.

2.5.4. Solid Characterization with FTIR

The infrared spectral data needed to determine the identity and quantity of the samples were obtained using a Varian 7000 FT-IR Spectrometer (Varian Inc., Palo Alto, California), 40 scans, 28,580 point per sample and 4 cm^{-1} resolution in the range of 4000 - 400 cm^{-1}. The instrument was purged for 30 min with nitrogen before analyzing the samples. The background was collected in the nitrogen atmosphere. After purging, ~5 mg of the solid was placed on the ATR crystal, the pressure arm was gently pressed on the sample so that the solid sample had good contact with the ATR crystal. No further preparation was required for analysis of melamine dendrons on the solid m-SiO_2. To analyze the results, the peaks of C-C (3500 - 2800 cm^{-1}) and aromatic (1800 - 1300 cm^{-1})

compounds were absorbed to check for presence of dendrons. The x and y values were then exported and graphed using Microsoft Excel. The graphs with negative y values were moved up by adding/subtracting values of the y value which was required for them to have positive y values. The graphs were overlaid at 1350 cm^{-1} to easily analyze the absorbance of each sample.

2.5.5. Ultraviolet Spectroscopy (UV)

UV-Visible spectroscopy is an instrumental scanning method that analyzes the absorption of UV light within the UV (200 - 400 nm) and visible (400 - 800 nm) spectrum. In the UV/vis region, molecules undergo electronic transitions from the ground state to the excited state. It is used to obtain the absorbance spectra of a compound in solution or solid state. UV/vis gives qualitative and quantitative imformation of highly conjugated organic compounds and biological molecules.

2.5.6. Film Characterization with UV

Ultraviolet spectroscopy (UV) was used to analyze the presence of dendrons in the films. The absorbance data for dendron films were obtained with an Olis Hewlett Packard (HP) 8452 Diode Array Ultraviolet Spectrophotometer, in the spectral range of 200 - 500 nm. No further preparation was required for the samples once the melamine dendrons were synthesized. The instrument was turned on for 30 min for the lamp to warm up before analyzing the samples. After 30 min, each film was analyzed by placing

the films to face the UV beam and taking spectra of each film at 200 - 500 nm. A background (films with amines only) was taken before each spectrum.

2.5.7. Film Properties: Contact Angle

Thickness and contact angle of the films were measured before and after calcification and also before and after coating with APTES. A KLA Tencor P-16 profilometer was used to measure thickness. Thickness of each film was taken three times at three different spot on the film and then the average of the three thicknesses was reported. A Ramé-Hart 100 Goniometer was used to measure water contact angle. Contact angle of each films were taken three times using 10 µL of distilled water placed in three different spots on the slides. The average of the three results was reported.

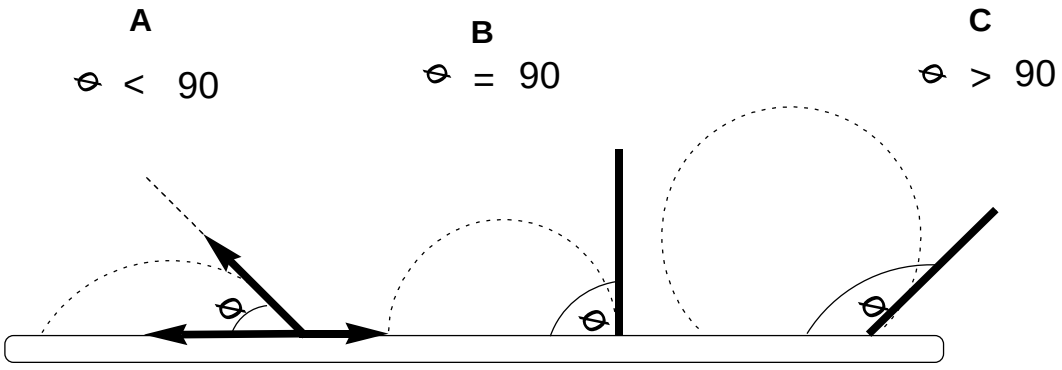

Figure 9. Illustration of measurement of water contact angle by determination of angle that water drops make on a surface: **(A)** high wetting $\theta < 90^{o}$ (hydrophilic), **(B)** intermediate wetting $\theta = 90^{o}$**;** and **(C)** low wetting $\theta > 90^{o}$ (hydrophobic).

Contact angle is measured at a liquid/vapor interface where the liquid meets a solid surface (here glass or silicon). A surface is hydrophilic if it tends to absorb water or be wetted by water. Wetted means that the liquid is spread evenly without the formation of droplets. If the contact angle of water is more than 30° and less 90° the surface is designated as hydrophilic. A surface is hydrophobic when the cohesive forces associated with the interaction between water and the surface are nearly equal the cohesive forces of bulk water. Advancing and receding contact angles were measured by slightly tilting the base of the goniometer. The advancing angles are measured for the downhill side and the receding angles are those measured on the uphill side of the droplet.

2.6. EXPOSURE TO VAPORS

2.6.1. 2, 4- Dinitrotoluene (DNT) Sensing

The m-SiO_2 dendron samples were placed in open glass vials and exposed to DNT vapor from a sample of DNT (7.25 mg) in a 50 mL Teflon jar with a screw cap lid for a timeframe ranging from 24 h to 72 h. Prior to inserting the sample in the chamber, the DNT was allowed to equilibrate for 24 h. UV, TGA or IR were used to check the presence of DNT. *Warning:* Although it is not an explosive like TNT, DNT is toxic and studies indicate that 2,4-DNT is readily adsorbed via oral or inhalation exposure and can be absorbed through skin in toxic amounts.[9]

CHAPTER 3

RESULTS AND DISCUSSION

3.1. SYNTHESIS OF MESOPOROUS MATERIAL

3.1.1. Sol-gel Synthesis

The substrate for the sensor is an SBA-15 type mesoporous silicate that has been well-described in the literature.[63] The Wirnsberger recipe using F-127 as a non-ionic surfactant templating agent[23] was used to form both solid and thin films using modifications developed in our laboratory. Starting with tetraethoxysilane, hydrochloric acid, F-127 and ethanol in 0.129: 23: 1: 1.4×10^3: molar ratios, the clear solution were formed after heating for one hour at reflux, then cooling to room temperature. The resulting sol-gel was used immediately for spin-coating films, or dried to a solid. The sol-gel remained as a solution for an extended period and was assumed to be stable for up to one week; we noticed that after one week precipitation sometimes to occur.

3.1.2 Film and Solid Mesoporous Silicates

Once the films were spin-coated, they were susceptible to cracking. Therefore they were dried slowly in a two-step procedure. First, the films were left overnight in a dessicator with high (100%) humidity. Then the films were calcined in a programmable furnace at a rate of 1 °C / min from room temperature up to 400 °C, left for 1 hour, then

again heated at 1 °C / min up to 600 °C and cooled. This procedure was developed through literature reports, the fact that F-127 decomposes rapidly between about 300 and 450 °C (Figure 8), and the observation that cracking occurred in films that were not heated slowly. Solids were dried in an oven at 80 °C, close to the boiling point of ethanol (86 °C), until visibly dessicated, then calcined using the same temperature program. Transmission electron microscopy showed that the solids and films were mesoporous, having 6 - 7 nm pores in a hexagonal structure.[72]

3.1.3. APTES Coating

3-Aminopropyltriethoxysilane (APTES) is the most commonly used organosilane coupling agent to prepare amino-terminated glass surfaces because the silane group can covalently bind to silicon or glass substrates.[73] The APTES-derivatized surfaces provide reactive amines to build up melamine-type dendrons on surfaces. The literature procedure[63] for SBA-15 derivatization with APTES resulted in a very low concentration (160 μL APTES for films and 800 μL APTES for solids) of amines on the surface, as evidenced by the small amounts of dendrons observed with TGA (see 3.5.2). Therefore, the films and solid surfaces reported here were derivatized with low (230 μL APTES for films and 1150 μL APTES for solids) and high (500 μL APTES for films and 500 μL APTES for 1.0 g m-SiO_2 solid) coverage of APTES. Low coverage coatings were accomplished by immersion of solid m-SiO_2 in a round-bottomed flask filled with

APTES (1 mmol) for 1 hour. The high concentration APTES treatment immersed for 24 h. For comparison, the usual approach in our research group for thin films is to use solutions of 1% APTES (4.2 mmol in 100 mL anhydrous toluene) for 15 min, which results in a monolayer or greater film thickness.[74]

3.1.4. Film Characterization

Mesoporous films were characterized with TEM, profilometry and goniometry after calcination and after APTES coating. All films were found to have a low contact angle after calcification, which indicates that the films were wetted (Table 2). This was expected because the surface has hydroxy groups available for hydrogen bonding with water.[75] After APTES coating the films had a higher contact angle with water, which indicates that the films are less hydrophilic due to the presence of hydrocarbons. An APTES-coated silicon surface has been reported to have advancing and receding contact angles from 51^{o} to 90^{o} and from 0^{o} to 33^{o}, respectively.[75]

Table 1. Contact Angles and Profilometric Thicknesses of m-SiO_2

Contact Angle (θ)				**Thickness (nm)**
After Calcification		**Before APTES**		**Profilometry**
θ_a (º) [a]	θ_r (º) [b]	θ_a (º)	θ_r (◦) [b]	433.8 ± 3.0
17 ± 2	15 ± 2	40 ± 2	30 ± 2	

[a]Advancing contact angle, [b]Receding contact angle. All the values are an average of three readings. The errors are the numbers between the average and high (+), and the average and the low (-).

3.2. SYNTHESIS OF DENDRONS AND IMINE DERIVATIVES

3.2.1 Synthesis of Dendrons

A synthesis of dendrons incorporating three different linking groups bound to m-SiO_2 solids was reported previously.[63] The synthesis of the composites using an AMP linker is shown in Figure 10. Starting with the APTES-coated solids, the surface-bound melamine dendrons were built iteratively in generations. The conditions for synthesis were based on the literature and all reactions were done at room temperature for 24 h.[63] The APTES-coated m-SiO_2 was treated first with cyanuric chloride (CC) to bind the dendron to the surface and provide a branch point for further generations. After rinsing thoroughly with CH_2Cl_2, THF, and MeOH to remove unreacted starting materials, the solids were treated with 0.4 M solution of 4-aminomethylpiperidine (AMP). The solids

were rinsed with three solvents again to remove unreacted starting materials. Although the AMP could potentially react at either the primary or secondary amine sites, literature[63] indicates that the secondary amine reacts faster, as expected from relative basicity. In model compounds synthesized using AMP as the linker molecule; a 10:1 ratio of products was obtained when reacted at 25 ^{o}C. The procedure was repeated again to build G2, then again to obtain G3.

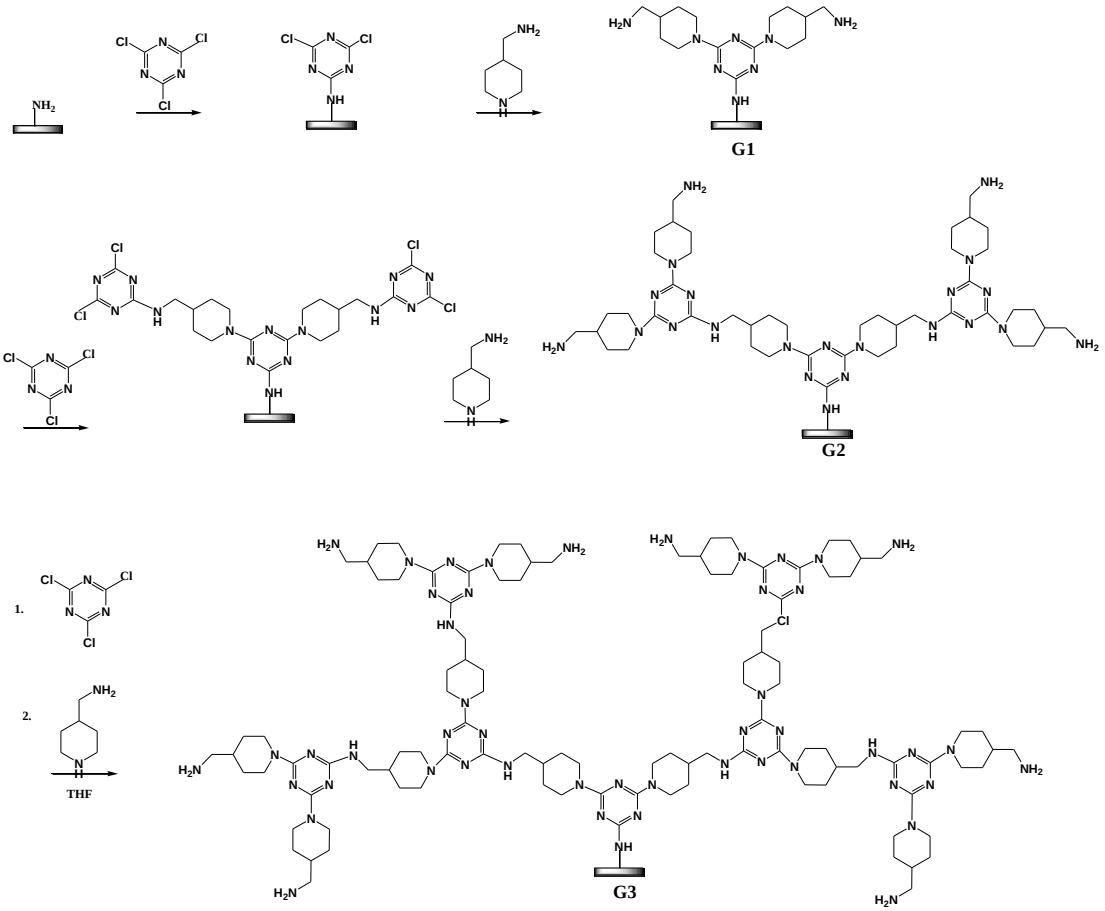

Figure 10. Synthesis of G1-G3 dendrons using linear synthesis.[63]

3.2. 2. Formation of the Imine Derivatives of Dendrons

Synthesis of the imine derivative of G1 was performed in order to provide a polar group to entrap DNT vapor (Figure 11). First, a model imine compound was synthesized using 4-aminomethylpiperidine and 3-hydroxybenzaldehyde (Figure 12). The model compound was originally synthesized in refluxing ethanol and reduced using $NaBH_3CN$.

However, when these standard conditions were used for solid-bound dendrons, only small amounts of organic material were detected by TGA at the imine stage, and extra inorganic material stuck to the m-SiO_2 substrate after reduction. Therefore, THF replaced EtOH as the solvent and the reaction was stopped at the imine stage (G1-imine).

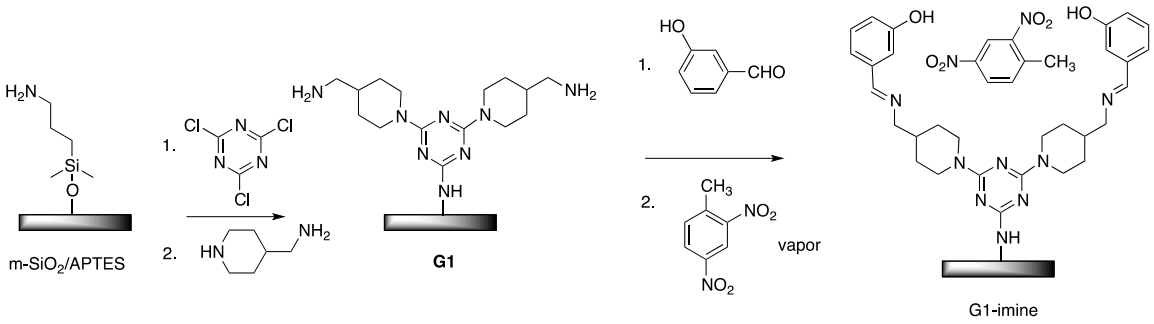

Figure 11. The imine derivative formation and proposed DNT detection.

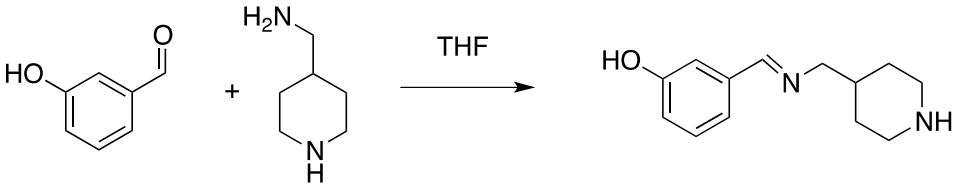

Figure 12. Model imine formation.

3.3. CHARACTERIZATION OF DENDRON STRUCTURES

3.3.1. Solid Characterization with TGA

Once the melamine dendron synthesis was completed, samples from each generation (G1-G3) were analyzed by TGA over the temperature range of 25 - 800 °C and representative runs are shown in Figure 13. The results show that a significant amount of total volatile and organic materials were removed thermally from the inorganic solid, providing indirect evidence of dendrons attached to the solids.

Weight losses for G1-G3 occurred in three regimes (Table 2). The first weight loss (**A**, 25 - 150 ºC) was assigned to loss of solvents, including water (bp 100 °C) from the m-SiO_2 because this loss was observed in all samples, even control samples containing no organic material. A second distinct weight loss range (**B**, 150 - 400 °C) was assigned to thermolysis of alkanes (C-C bonds) and accounted for about 10% loss. Finally, a third region of weight loss, **C**, was identified between 400 - 800 ºC. This was assigned to the decomposition of residual aromatic rings (C=C bonds) and amounted to 3% of the total weight. At around 750 °C, the organic material was assumed to be completely removed from the inorganic m-SiO_2.

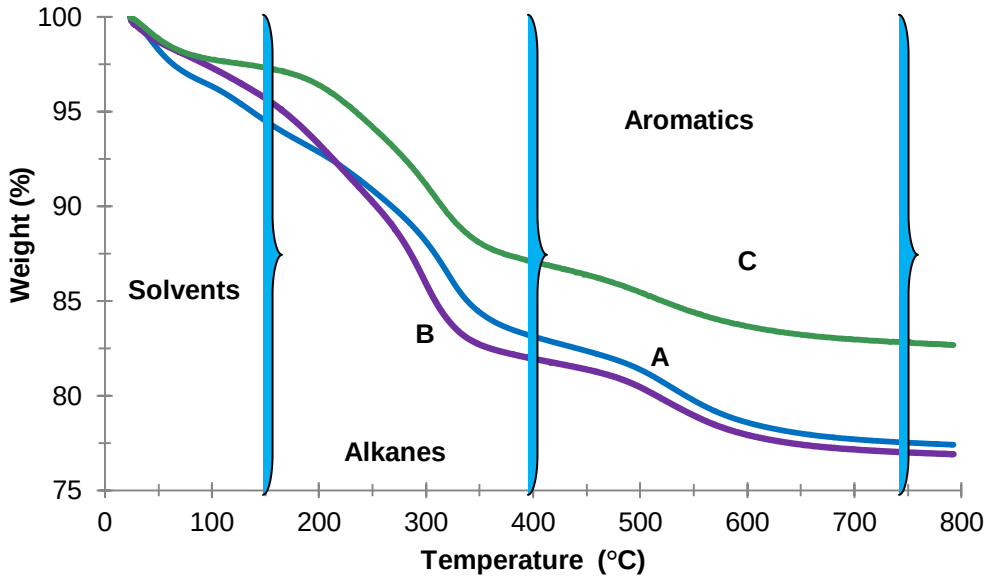

Figure 13. Thermogravimetric analysis results for the solid-bound dendron samples formed under reaction conditions designed to give three generations: **A**) G1 (blue line); **B**) G2 (purple line); and **C**) G3 (green line).

Bonds between oxygen and silicon (amine coating bond to m-SiO_2) are quite strong (110 kcal/mol), therefore cleavage of dendrons from the m-SiO_2 surface during reaction conditions used to synthesize or rinse the dendrons was not expected. The TGA data showing that minimal organic material was added beyond G1 indicates that further generations were not formed, perhaps due to insufficient heat to complete the reactions at each step.[76] The small overall weight losses in G2 and G3 relative to G1 may result from removal of entrapped reagents from pores during the extensive washing because the amounts are still within experimental error of losses expected for G1. G1 had the greatest

amount of solvents associated with the dendrons, followed by samples originally thought to be G2 and G3. G1 may be expected to have the greatest affinity for polar solvents because exposed m-SiO_2 (or primary amine functional groups in the APTES coating) could retain polar solvents and hydrogen-bond to water. G3 would be expected to retain solvents least readily - but losses in ranges **A-C** for samples labeled G3 look very similar to those in G1. If the dendrons are limited to G1, subsequent treatments with dendron-building reagents might improve the quality of the G1 dendron, thus blocking the surface better and adding organic material in TGA loss ranges **B** and **C**. Indeed, the samples labeled G2 had greater losses in range **B** (150 - 400 ºC) compared to G1 and G3.

Table 2. TGA for Dendronic Solids with Low Concentration Amine Coating

Samples	A (25 - 150°C)	B (150 - 400°C)	C (400- 750°C)	Total % loss
	1st % loss	2nd % loss	3rd % loss	
Control (m-SiO_2)	9.1	1.5	-	11 [a]
Amine Coated m-SiO_2 (G0) (3.4 mmol APTES 0.68 mmol/g*)	3.6	1.5	1.7	7 [a] , 3 [b] 5 [c]
G1	3.7	12	5.4	21 [a], 17 [b] 11[c]
G2	1.7	13	4.7	19 [a], 17[b] 20 [c]
G3	2.5	10	4.5	18 [a] , 16)[b] 31 [c]

[a] Each weight loss value is an average of three data points. The TGA results from the current study; [b]Solvent weight loss subtracted from total weight loss in current study; [c] literature values[63] for APTES treated m-SiO_2 (0.5 mmol /g).

TGA of amine-coated solids showed comparable percent weight losses (7%) compared to the weight losses reported in the literature (5%).[63] The total weight losses in Table 2 were originally assumed to be for different generations (G1-G3), although we also expected a slight increase in the total % losses as compared to literature since our

amine concentration was larger 0.68 mmol vs. 0.5 mmol. It is not clear whether the literature values included losses due to solvent. Since the total % losses were lower than expected, we concluded that G1 was the only dendron generation formed. Poor amine coverage may have resulted from misinformation in the published description of amine coating. Careful reading of the supplementary documentation[63] revealed that 3-aminopropyl trimethoxysilane (APTMS) was used, yet APTES was reported, resulting in a difference of 33% in the amount of amine functional groups available.

According to the literature,[63] the amount of organic material in the dendrons should increase by ~10% TGA weight loss at each generation (G0 = 5, G1 = 11, G2 = 20, G3 = 31). However, as shown in Table 2, the generations appear to stop growing at G1 and even undergo small losses in higher generations (G0 = 7, G1 = 21, G2 = 20, G3 = 18). Therefore we increased APTES concentrations to 2.1 mmol / g m-SiO_2 to increase number of sites for dendron growth. The total % loss values shown in Table 3 indicate that even though the weight loss for G1 matched literature at 0.5 mmol APTES / g of m-SiO_2 (11%), and the amount of dendrons increased for each generation, the total weight losses fell short of those reported in the literature for G3 (38%) by 16%.

Table 3. TGA for Dendronic Solids with High Concentration Amine Coating

Samples	**A(25 – 150 C)**	**B(150 – 400 C)**	**C(400 – 750)**	**Total % loss**
	1st % loss	**2nd % loss**	**3rd % loss**	
Amine -Coated m-SiO_2 (G0) (0.5 % APTES, 2.1 mmol / g)	5.8	2.9	-	9[a] , 3[b] 5[c] , 8[d]
G1	7.2	6.5	4.4	18[a] , 11[b] 11[c]
G2	6.8	7.5	8.4	23[a] , 16[b] 20[c]
G3	4.1	9.6	12	26[a] 22[b] 31[c] , 38[d]

[a]The TGA results from the high concentration APTES (2.1 mmol/g); [b]Solvent weight loss subtracted from current study; [c] literature values[63] for APTES treated m-SiO_2 (0.5 mmol /g); [d] Literature values[63] for weight losses on APTES treated m-SiO_2 (1.0 mmol / 100 mL) .

The literature reported the 8% weight loss for G0 and 38% weight loss for G3 for 1.0 mmol of APTES / g amine loading, but did not mention total weight losses for G1 and G2. If we assume that the literature values do not include solvents, the experimental values are close to the expected weight losses for G1 at lower amine loadings, and G2

may have been formed at the stage where G3 was expected, but the formation of G3 is not supported by the evidence.

3.3.2. Characterization of Imine Derivatives with TGA

The G1 solids from Table 2 were initially reacted with 3-hydroxybenzaldehyde in refluxing methanol, the classic solvent used for imine formation. These reaction conditions removed most of the dendrons from the solids leaving 2% organic material. The successful model reaction between 3-hydroxybenzaldehyde and 4-aminomethylpiperidine showed that refluxing THF solvent does support imine formation. Therefore, G1 samples from Table 2 were reacted with excess 3-hydroxybenzaldehyde for 1 hour. Comparing to G1, the overall weight loss in G1-imine was expected to increase by 30% (~5% based on G1, for a new weight loss value of 22%) due to the larger amount of organic material that could be lost upon C-C bond breakage in imine derivatives. G1 from Table 3 was expected to increase by 30% upon conversion to imine, adding 3% of total organic weight in G1-imine, for a new weight loss value of 14%.

The experimental weight losses for the imine derivatives are shown in Table 4. The overall weight % *decreased* by ~1% for each sample relative to dendron-coated solids identified as G1 in Table 2, when solvent weight losses were subtracted. However, for the G1 derivative in Table 3, the loss *increased* by 5% after solvent loss was subtracted, 2% more than the calculated expectation value of 14%.

Table 4. TGA for Imine Derivatives

Source of G1	**A (25 - 150°C)**	**B (150 - 400°C)**	**C (400- 750°C)**	**Total % loss**
	1st % loss	**2nd % loss**	**3rd % loss**	
Run 1: G1[a]	1.6	11	5.3	18, 16[c]
Run 2: G1[a]	1.4	12	4.6	18, 16[c]
Run 3: G1[a]	2.1	13	4.1	19, 17[c]
G1[b]	5.2	5.2	10	21, 16[c]

[a] G1 was formed on low load amine m-SiO_2 after 1 hour reflux; [b] G1 was formed on high load amine m-SiO_2 after 8 h reflux; [c] Values reported with solvent loss subtracted.

The apparent lack of reaction to imine in the Table 2 G1 samples may be due to the low concentration of 3-hydroxybenzaldehyde and short reaction time used in conversion. The loss, rather than gain, of organic material during reaction may be attributed to removal of any unreacted starting materials stuck in pores in refluxing THF. The G1 formed on high load amine-coated m-SiO_2 appears to have formed the imine derivative because the organic weight percent increased as expected. The fact that the increase was more than expected my be due to the presence of unreacted primary amine functional groups at the the solid surface that also formed imines. This side reaction apparently did not take place

with the G1 dendons because the milder reaction conditions were not sufficient to derivatize the crowded surface.

3.3.3. Characterization of Dendronic Films with UV Spectroscopy

Ultraviolet spectroscopy (UV) was used to analyze the presence of dendrons in the films. The m-SiO_2 films coated with APTES were used as a control while the dendron coated films were analyzed. Since m-SiO_2 is UV-transparent, the UV results showed presence of dendrons through the absorbance of the triazine ring in the films at different generations (Figure 15). For the first generation (G1) the absorbance was ~0.3 and it doubled with the second generation (G2) to ~0.6. The absorbance of G3 decreased below the first generation to ~0.15. This absorbance trend was seen in every UV of the film. Variation in absorbance is likely not affected by variations in film thicknesses because of the transparency of the films and the fact that dendrons mostly on the surface and are unlikely to grow in pores deep in the films. It is unclear why the absorbance of G3 films could be lower than its precursor G2. One explanation is that dendrons become crowded the higher the generation, requiring longer reactions times and higher temperatures.

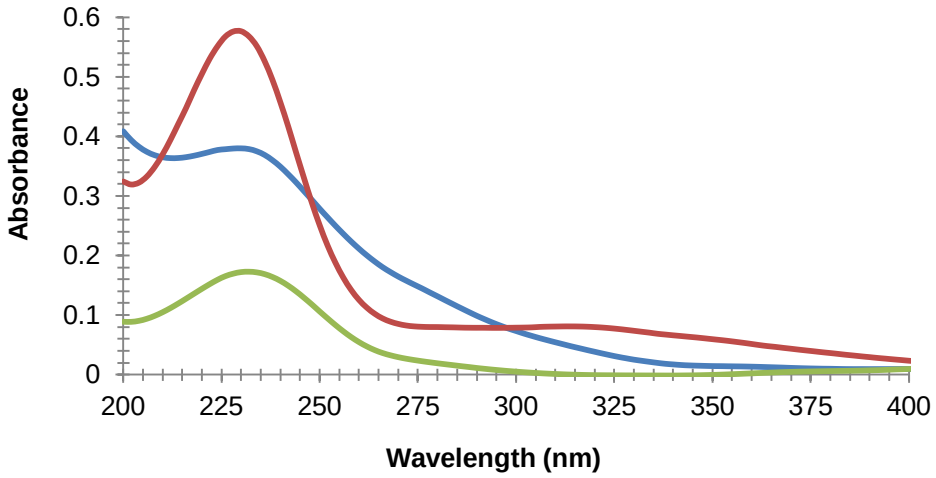

Figure 14. UV Spectra of dendron thin films at generations G1 (blue), G2 (red) and G3 (green).

The temperature at which the dendrons were synthesized was relatively low and the length of time short. A literature report [62] indicated that synthesis of some higher order dendrons can take days or even a week, while we synthesized the G1 dendron films at 40 °C for 24 hours each step. However, due to the fact that the UV of dendrons (λ_{max} = 234 nm) appears in the same region as DNT (λ_{max} = 252 nm) in a thin film (Figure 15), UV was not the ideal spectroscopic method for characterization.

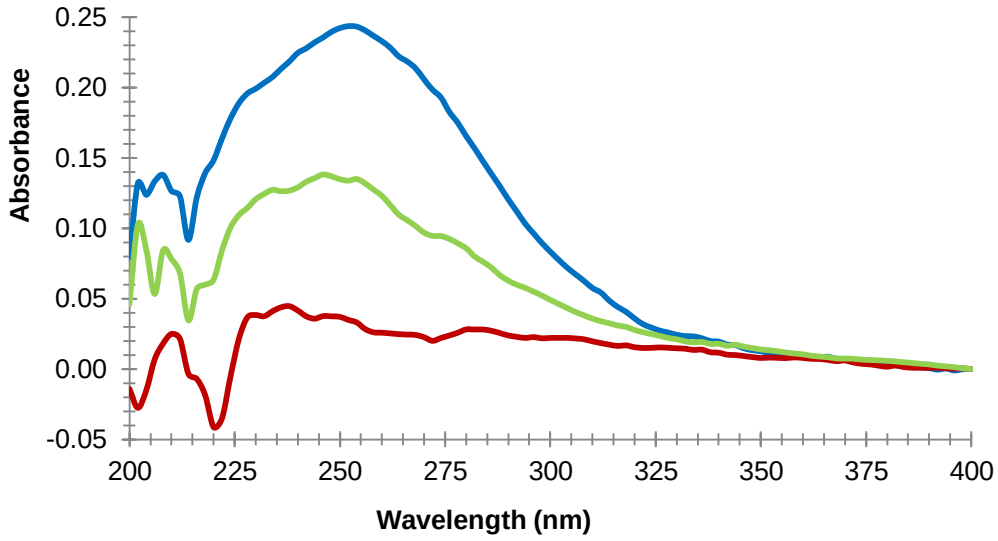

Figure 15. UV spectra for on organically modified SiO_2 film imprinted with DNT (blue line), after Soxhlet extraction with methanol (red line), and after exposure to DNT vapor (green line).

3.3.4 Solid Characterization with FTIR

FTIR was used to further analyze the solids to identify them for the presence of certain functional groups. The solids were not quantitatively analyzed because the same amount of solid was not compared between samples.

The FTIR spectra of dendron-coated solids (assumed to be generations G1-G3) showed three distinguishing peaks (Figure 16): peaks **A** are assigned to C-N bond stretching in amines; **B** to the aromatic ring C=C stretching (1700 - 1400 cm^{-1}), and **D**

(3000- 2800 cm^{-1}) is assigned to alkane C-H bond stretching and (3100-3000) from Csp^2 - H bond stretching.

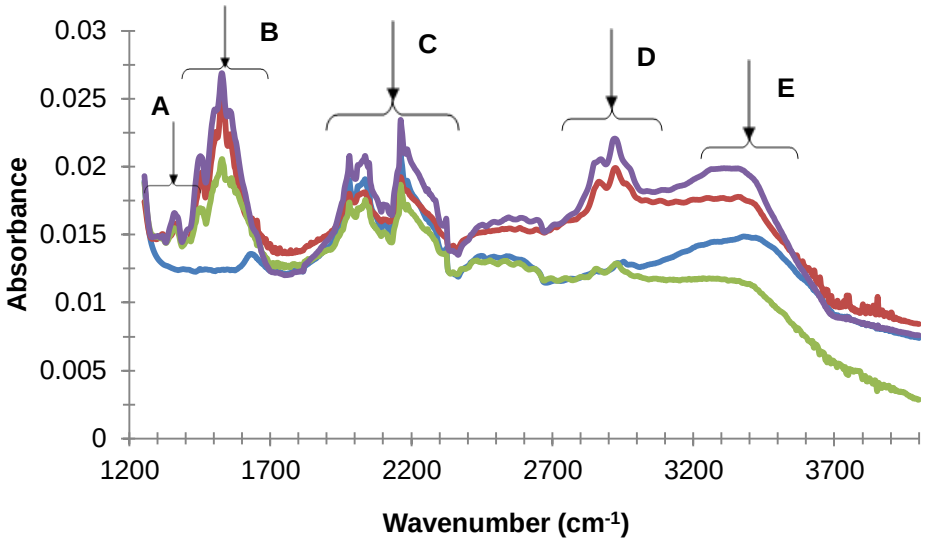

Figure 16. IR spectra of amine-coated m-SiO_2 (blue) and G1 (red), G2 (green) and G3 (purple) on m-SiO_2 solids.

The broad peak at **E** (3600 - 3200 cm^{-1}) is presumably due to N-H stretching and/or water associated with the solids. The large peaks at **C** are artifacts due to the diamond ATR crystal. Only solid samples were analyzed using the FTIR because film samples needed a gold coating, and the films often peeled off gold-coated silicon substrates.

3.4. Binding of DNT to Dendrons

3.4.1. Model Compounds

Equilibrium geometries for surface-bound dendrons were modeled using HF (3-21G* and 6-31G**). A methyl amino group was connected to the G1 structure to simulate the 3-aminopropyl triethoxysilane coating attached to the m-SiO_2 surface. The G1 dendron was built such that the bonds connecting the piperidine ring were both equatorial and the primary amines on the dendron periphery were oriented upward rather than outward. The dendron was built and energy minimized with AM1 before forming imine (G1-imine) from 3-hydroxybenzaldehyde. The functionalized dendron (G1-imine) was then minimized. Finally, a DNT molecule was added to simulate dendron vapor adsorption.

The minimizations of G1-imine with DNT showed three orientations that resulted in local minima. In each, the H-bonding interactions between the phenol proton and the nitro group oxygens are strong, with interatomic distances between 1.9 and 2.5 Å (Table 5). depending upon equilibrium geometry and basis set used.

Table 5. Calculations of Hydrogen Bonding Distances Between O in Each Nitro Group of DNT and Both Phenol Protons

Model	**3-21G* (Å)**	**6-31G** (Å)**
GI-imine-DNT1	1.903, 1.968	2.134, 2.531
GI-imine-DNT2	1.916, 2.004	*n/a*
G1-imine-DNT3	2.187, 2.177	2.121, 2.143

In one favorable G1-imine-DNT interaction, the DNT methyl group was pointing into the interior of the hydrophobic cavity of the dendron (G1-imine-DNT2, Figure 17). This allowed the interaction of an oxygen atom on each nitro group to interact with both G1-imine phenol protons.

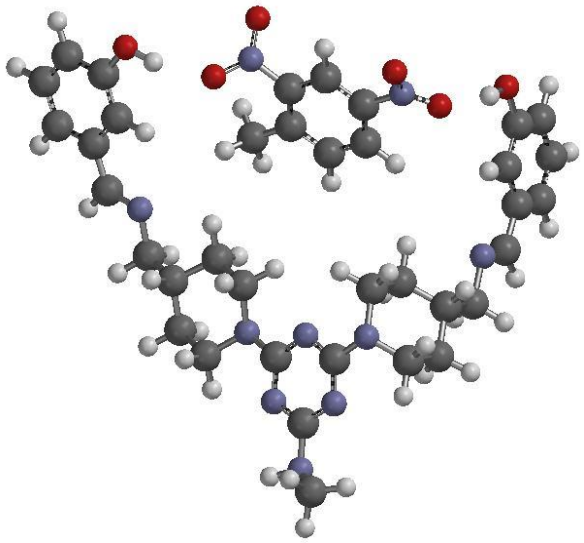

Figure 17. Calculated model of DNT interaction with G1-imine.

Calculations predicted that another favorable interaction between DNT and G1-imine can take place. This is an electrostatic attraction between the electron-deficient nitro group and the electron-rich amine in piperidine. Although π-π interactions are not part of standard calculations in PC Spartan, these attractive forces would be expected to further lower the energy of interaction between DNT and the G1-imine dendrons.

In G1-DNT, inter-ring interactions *and* H-bonding were predicted. The inter-ring distances between electron-rich and electron-poor nitrogens ranged from 5.0 to 5.5 Å and H-bonding distances in G1-DNT were 2.4-2.7 Å. In contrast, inter-ring interactions were stronger (4.2-4.8 Å) yet simultaneous H-bonding was not possible in G1-imine-DNT.

Table 6. Hartree-Fock 3-21G* Calculations of Distance between DNT and Dendron Piperidine Nitrogens.

Model	Inter-ring (Å)	H-bonding (Å)
GI- DNT	5.534, 4.595	2.692, 2.443
GI-imine-DNT	4.798, 4.200	n/a

3.4.2. DNT Vapor Exposure

The G1 solids that underwent unsuccessful attempted conversion to imines were exposed to DNT vapor for 24 hours. Adsorbed DNT was expected to show an increase in the first percent weight loss, since the TGA weight loss of DNT occurred at 97 °C and DNT does not covalently bond to dendrons. A small 1.4-2.1 % weight loss was observed at 25 - 150 °C in all three G1 samples. (Table 7). The G1-imine derivative from the high amine loaded m-SiO_2 (Table 8) showed an increase in first % weight loss, but this was

accompanied by unexplained loss in the second weight loss and gain in third. TGA results were inconclusive evidence for DNT adsorption.

3.4.3. TGA Characterization of DNT Binding

Table 7. TGA after Exposure of G1 Solids to DNT

Derivative	**A (25 - 150°C)**	**B (150 - 400°C)**	**C (400- 750°C)**	**Total % loss**
	1st %loss	**2nd %loss**	**3rd %loss**	
G1	2.1	11	4.9	18
G1	1.6	12	4.3	18
G1	1.4	11	3.9	16

Table 8. TGA of G1- Imine Derivative Before and After DNT Exposure

Derivative	**A (25 - 150°C)**	**B (150 - 400°C)**	**C (400- 750°C)**	**Total % loss**
	1st % loss	**2nd % loss**	**3rd % loss**	
G1-imine	2.7	6.2	7.0	16
G1-imine (+DNT)	4.5	4.8	9.5	19

3.4.4. UV Spectrum after DNT Exposure

The λ_{max} of the dendronic solids overlaps with the λ_{max} of DNT vapor. In previous research, UV λ_{max} of DNT was found to be ~252 nm when entrapped in a hybrid organosiloxane film.[77] Figure 14 shows that the λ_{max} for dendron films shifts with generation ranging from 232 nm for G1, to 234 nm for G3, and red-shifted (λ_{max} = 240 nm) for G2. Since the λ_{max} for DNT and dendron films are close to each other, the one way to tell whether there was DNT present in the films with dendrons was to check for any increase or decrease in the absorbance values for the films. The UV spectrum in Figure 18 shows inconclusive effects of exposure to DNT after 1 to 3 days. Although the dendron surfaces developed a shoulder tailing into the visible region (λ_{max}= 320 nm), that absorbance does not appear to be associated with DNT.

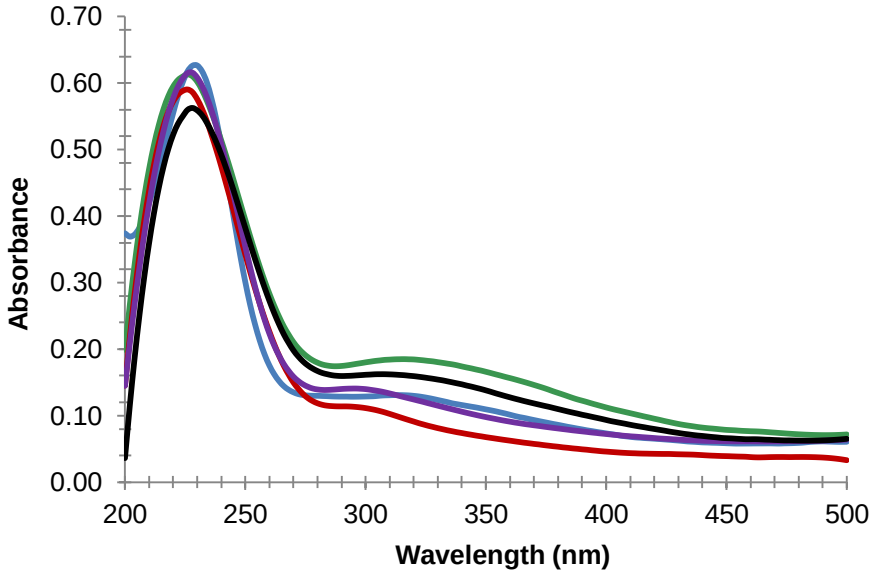

Figure 18. UV spectrum of G2 dendron surfaces (blue); modified to the imine (green); after 24 h exposure to DNT (red); 48 h exposure to DNT (purple), and 72 h exposure to DNT (black).

3.4.5. IR Spectrum after DNT Binding

An IR spectrum of 97 % DNT solid was analyzed to check DNT peaks (Figure 19). The IR spectra showed two distinguishing peaks, two in the region at **A** (~1300 and 1500 cm^{-1}) for the N-O stretch in the nitro groups, **B** (1775 - 2275 cm^{-1}), an artifact of the ATR crystal, and **C** (3100 cm^{-1}) due to aromatic C-H stretches.

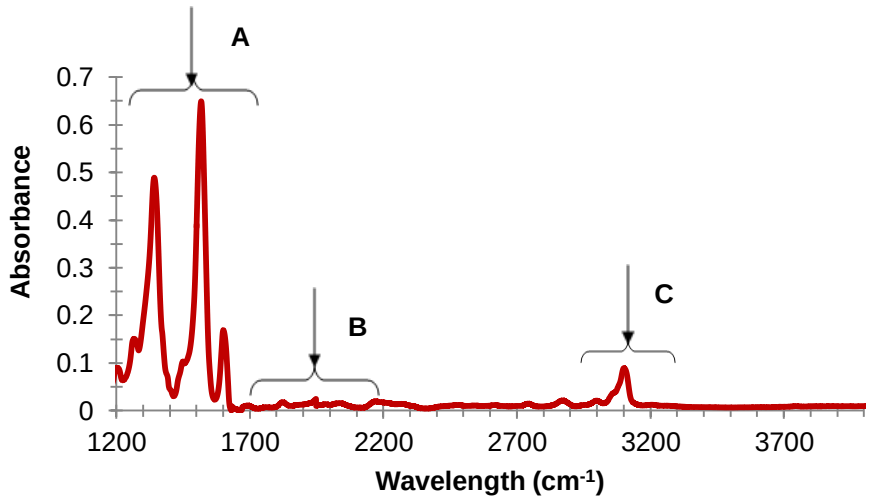

Figure 19. IR Spectrum of solid DNT.

Control spectra were taken to check the affinity of DNT vapors for the solids without dendrons (Figure 20). APTES-coated and uncoated m-SiO_2 were exposed to DNT for 24 hours. By comparison with the authentic DNT spectrum (Figure 19), the absence of peaks at **A** and **C** indicate that DNT is not present.

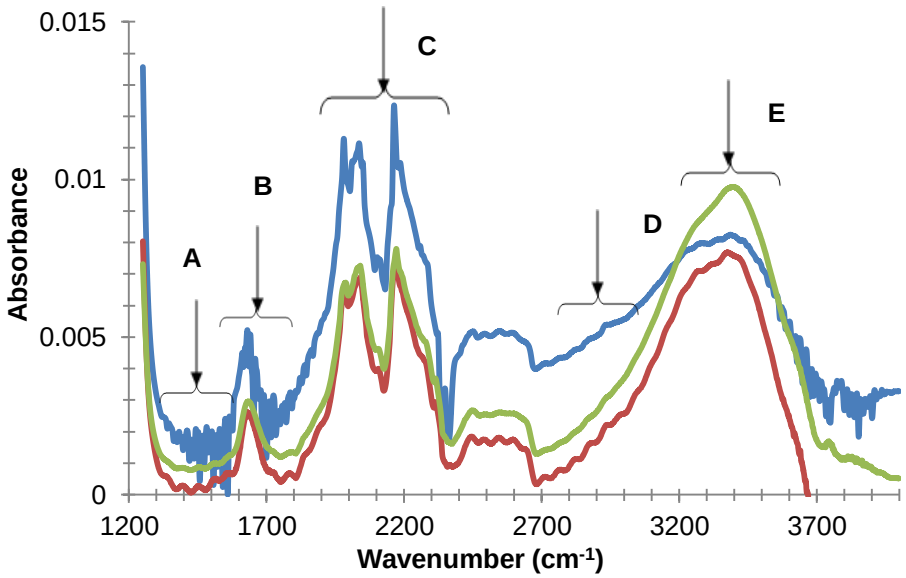

Figure 20. IR spectra of solid controls; amines (blue line), amines + DNT (red line), and SiO_2 + DNT (green line)

Figure 21 shows a G1-derivatized surface before and after exposure to DNT vapor. The G1 solid has the expected strong absorbances in the **B** (1700 - 1400 cm^{-1}) region due to the melamine aromatic stretching, and N-H stretching at **E**, although the C-H stretching at **D** is not as pronounced as in Figure 16. DNT nitro absorbances are not detectable at 1300 and 1500 cm^{-1}. This outcome does not indicate an increased affinity of DNT for the G1-modified surface as compared to the control samples in Figure 20. It is possible that the N-O stretching bands in DNT may shift when DNT adsorbs on G1 solids such that it is not distinguishable from the aromatic C=C stretching in region **B**.

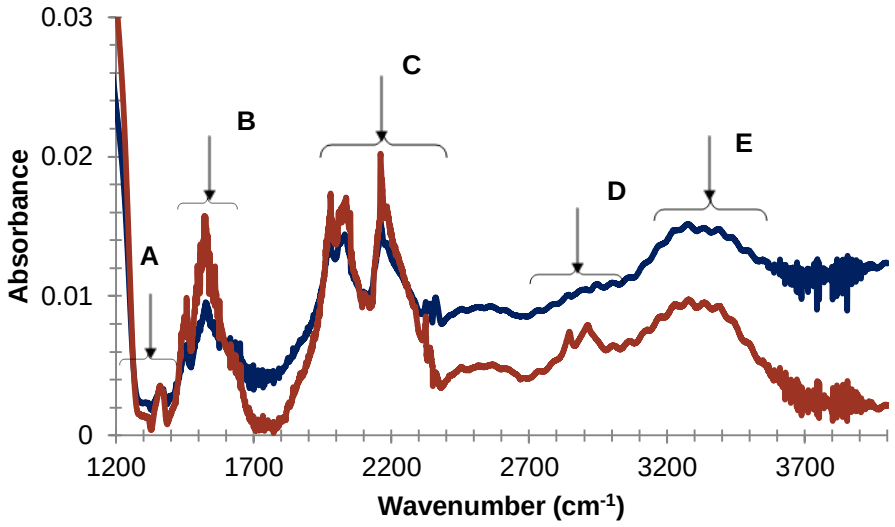

Figure 21. IR spectra of G1-derivatized solid before (navy blue line) and after (brown line) 24 hours DNT exposure.

CHAPTER 4

CONCLUSIONS

A solid composed of inorganic mesoporous SiO_2 material coated with one generation (G1) of melamine dendrons was synthesized in a modification of a literature procedure.[63] The quanification of organic dendrons formed on solid inorganic m-SiO_2 was assessed using TGA weight % losses. The TGA measurements indicated that G1 was formed (11-17% overall weight loss, correcting for adsorbed solvents) by comparison to literature values for G1 (11%), G2 (20%) and G3 (31%).[63] Attempts to build subsequent generations on m-SiO_2 solids still resulted in G1 or an incomplete G2 layer. The organic loading due to dendrons was found to depend on the concentration of APTES used in formation of the amine coating. Lower loading (7% weight loss) resulted in G1 only, whereas higher amine loading (9%) and literature (8-10%)[63] resulted in more G2. The proposed reasons for the differences could be that the reaction conditions were insufficient to complete the reaction in subsequent dendron generations,[76] although room temperature reactions were reported in literature for dendrons G1- G3 on solids. Further, the pore sizes for the dendronic solids were in the range of 6 -7 nm, which is a tight fit for larger dendrons (G3 is ~4 nm wide at the outer edge when it forms a cone-shaped dendron) whereas literature m-SiO_2 had ~8 nm pore sizes. Also, the large number of rinses and mechanical processes necessary for interactive synthesis of surface-bound

dendrons could remove the organic material from the surface especially for larger dendron generations. FTIR showed the presence of dendrons in the solids, as compared to uncoated and amine-coated silica, but amounts of dendrons could not be quantified.

A model imine was prepared easily from 4-aminomethylpiperidine and 3-hydroxybenzaldehyde in THF. However, treatment of m-SiO_2 - G1 with 3-hydroxybenzaldehyde under the same conditions did not result in imine formation. Dendrons were also built on m-SiO_2 films. Films showed an unexpected but reproducible trend in dendron loading G3< G1 < G2 by UV spectroscopy. The films were fragile and were observed to peel off the surface after repeated rinsing. The imine-derivatized films showed an overall decrease in the UV absorbance at 250 nm as compared to melamine dendrons, presumably due to removal of organic material from the surface due to rinsing in hot THF.

Calculations predict that G1-imine dendrons should have greater affinity for DNT than G1 based on strong H-bonding interactions of nitro group oxygens with the phenol hydrogen. Computational models also demonstrated that G1 undergoes π-π stacking interactions with DNT due to two interactions between electron-deficient nitro group nitrogens and electron-rich piperidine nitrogens.

DNT was expected to be spectroscopically distinguishable from dendrons and imine derivatives due to nitro N-O stretches at 1300 and 1500 cm^{-1}. However, when exposed to DNT vapors, these stretches were not observed in G1 or control samples. It is

noteworthy that UV spectroscopy could not readily distinguish the DNT analyte from the imine derivative either, because all three materials absorb in the same UV wavelength range.

In summary, first generation (G1) melamine dendrons were built on solid and film mesoporous silicates and conditions for imine derivative formation established. Calculations predicted that G1-imine solid should have a high affinity for DNT vapor through H-bonding at the dendron surface and electrostatic attractions in the interior of the dendron. G1 dendrons are predicted to have both π-π stacking and electrostatic attraction to DNT. However, binding of DNT was not observed spectroscopically in G1. Future work will focus upon synthesis of G1 and G1-imine on m-SiO_2 solids. The solids will be exposed to DNT and analyzed by IR, and compared.

REFERENCES

1. Tang, Z.; Song, Y.; Tian, Y.; Liu, L.; Guo, Q. Effects of Surfactant on the Pore Structure of Mesoporous Carbon. *Microporous Mesoporous Mater.* **2008,** *11*, 48-54.
2. Jin, G.W.; Koo, H.; Nam, K.; Kim, H.; Lee, S.; Park, J.S.; Lee, Y. PAMAM dendrimers with a 1,2-Diaminoethane Surface Facilitates Endosomal Escape for Enhanced pDNA Delivery. *Polymer* **2001,** *52*, 339-346.
3. Albertazzi, L.; Storti, B.; Marchetti. ; Beltram. Delivery and Subcellular Targeting of Dendrimer-Based Fluorescent pH Sensors in Living Cells. *J. Am. Chem. Soc.* **2010,** *132*, 18158-18167.
4. Jansen, J. F. G. A.; Brabender-Van den Berg, E. M. M.; Meijer, E. W. Encapsulation of Guest Molecules into a Dendritic Box. *Science* **1994**, *266*, 1226-1229.
5. Scott, B. J.; Wirnsberger, G.; Stucky, G. D. Mesoporous and Mesostructured Materials for Optical Applications. *Chem. Mater*. **2001**, *13*, 3140-3150.
6. Dancil, K. P. S.; Greiner, D. P.; Sailor, M. J. A Porous Silicon Optical Biosensor: Detection of Reversible Binding of IgG to a Protein A-Modified Surface. *J. Am. Chem*. Soc. **1999**, *121*, 7925-7930.

7. Yoh, J. J.; McClelland, M. A.; Maienschein, J. L.; Wardell, J. F.; Tarver, C. M. Simulating Thermal Explosion of Cyclotrimethylenetrinitramine-base Explosives: Model Comparison with Experiment. *J. Appl. Phys*. **2005,** *97*, 083-504.
8. Chen, Z.; Foster, M. W.; Zhang, J.; Mao, L.; Rockman, H. A.; Kawamoto, T.; Kitagawa, K.; Nakayama, K.; Hess, D. T.; Stamler, J. S. An Essential Role for Mitochondrial Aldehyde Dehydrogenase in Nitroglycerin Bioactivation. *Proc. Natl. Acad Sci.* **2005,** *102*, 12159-12164.
9. Lenz, A.; Pohl, A.; Ojamae, L.; Persson, P. Computational Study of the Catalytic Effect of Platinum on the Decomposition of DNT. *Intl. J. Quantum Chem.* **2012,** *112*, 1852-1858.
10. Johnson, G. R.; Jain, R. K.; Spain J. C. Origins of the 2,4-Dinitrotoluene Pathway. *J. Bacteriol.* **2002,** *184*, 4219-4232.
11. Jang, J.; Bae, J. Fabrication of Mesoporous Polymer / Silica Hybrid Using Surfactant-Mediated Sol-gel Method. *J. Non-Crystalline Solids* **2006**, *352*, 3979-3984.
12. Gan, W. Y.; Lee, M. W.; Amal, R. Photoelectrocatalytic Activity of Mesoporous TiO_2 Films Prepared Using Sol-gel Method with Tri-block Copolymer as Structured Directing Agent. *J. Appl. Electrochem.* **2008**, *38*, 703-712.
13. Medle, B. J.; Johnson, B. J.; Charles, P. T. Mesoporous Silicate Materials in Sensing. *Sensors* **2008**, *8*, 5202-5228.

14. Scott, B. J.; Wirnsberger, G.; Stucky, G. D. Mesoporous and Mesostructred Materials for Optical Applications. *Chem. Mater.* **2001,** *13,* 3140-3150.

15. Fryxell, G. E. The Synthesis of functional Mesoporous Materials. *Inorg. Chem. Commun*. **2006,** *9,* 1141-1150.

16. Boissiere, C. ; Grosso, D.; Lepoutre, S.; Nicole, L.; Bruneau, A. B.; Sanchez, C. Porosity and Mechanical Properties of Mesoporous Thin Films Assessed by Environmental Ellipsometric Porosimetry. *Langmuir* **2005**, *21,* 12362-12371.

17. Yamada, T.; Zhou, H.; Tomita, M.; Ueno, Y.; Ichio, T.; Honma, I.; Asai, K.; Katsube, T. Surface Photovoltage NO Gas Sensor with Properties Dependent on the Structure of the Self-ordered Mesoporous Silicate Film. *Adv. Mater*. **2002**, *14*, 812-815.

18. Johnson, J. A.; Finn, J. M. G.; Koberstein, J. F.; Turro, N. J. Construction of Linear Polymers, Dendrimers, Networks, and Other Polymeric Architectures by Copper-Catalyzed Azide-Alkyne Cycloaddition “Click” Chemistry. *Macromolecular J.* **2008,** *29,* 1052-1072.

19. Bagshaw, S. A.; Prouzet, E.; Pinnavaia, T. J. Templating of Mesoporous Molecular Sieves by Nonionic Polyethylene Oxide Surfactants. *Science* **1995**, *269*, 1242-1244.

20. Zhao, D.; Feng, J.; Huo, Q.; Melosh, N.; Fredrickson, G. H.; Chmelka, B. F.; Stucky, G. D. Triblock Copolymer Syntheses of Mesoporous Silica with Periodic 50 to 300 Angstrom Pores. *Science* **1998**, *279*, 548-552.
21. Zhao, D.; Huo, Q.; Feng, J.; Chmelka, B. F.; Stucky, G. D. Nonionic Triblock and Star Diblock Copolymer and Oligomeric Surfactant Syntheses of Highly Ordered, Hydrothermally Stable, Mesoporous Silica Structures. *J. Am. Chem. Soc.* **1998,** *120*, 6024-6036.
22. Zhao, D.; Feng, J.; Huo, Q.; Melosh, N.; Fredrickson, G. H.; Chmelka, B. F.; Stucky. G. D. Triblock Copolymer Syntheses of Mesoporous Silica with Periodic 50 to 300 Angstom Pores. *Science* **1998,** *279,* 548-550.
23. Wirnsberger, G.; Scott, B. J.; Stucky, G. D. PH Sensing with Mesoporous Thin Films. *Chem. Commun.* **2000,** 119-120.
24. Swager, T. M.; Yang, J. S. Porous Shape-Persistent Fluorescent Polymer Films: An Approach to TNT Sensory Materials. *J. Am. Chem. Soc.* **1998,** *120,* 5321-5322.
25. Sarkar, K.; Salinas, Y.; Campos, I.; Martinez-Manez, R.; Marco, M. D.; Sancernon, F.; Amoros, P. Organic–Inorganic Hybrid Mesoporous Materials as Regenerable Sensing Systems for the Recognition of Nitroaromatic Explosives. *CHEMPLUSCHEM*, **2013***, 78*, 684-694.

26. Vu, A.; Phillips, J.; Bühlmann, P.; Stein, A. Quenching Performance of Surfactant-containing and Surfactant-free Fluorophore-doped Mesoporous Silica Films for Nitroaromatic Compound Detection. *Chem. Mater.* **2013**, *25*, 711-722.

27. Hayder, M.; Fruchon, S.; Fournie, J. J.; Poupot, M.; Poupot, R. Anti-Inflammatory Properties of Dendrimers per se. *Sci. World J.* **2011,** *11,* 1367-1382.

28. Tao, S.; Li, G. Porphyrin-doped Mesoporous Silica Films for Rapid TNT Detection. *Coll. Poly. Sci*. **2007**, *285,* 721-728.

29. Tao, S.; Lo, G.; Zhu, H. Metalloporphyrins as Sensing Elements for the Rapid Detection of TNT Vapor. *J. Mater. Chem.* **2006,** *16,* 4521-4528.

30. Fu, X-C.; Chen, X.; Wang, J.; Lui, J-H.; Huang, X-J. Amine Functionalized Mesoporous Silica Microspheres with Perpendicularly Aligned Mesopore Channels for Electrochemical Detection of Trace 2-4,6-Trinitrotoluene. *Electrochim. Acta* **2010**, *56,* 102-107.

31. Shi, G.Y.; Qu, Y.H.; Zhai, Y.Y.; Lui, Y.; Sun, Z.Y.; Yang, J.G.; Jin, L.T. {MSU/PDDA}*n* LBL Assembled Modified Sensor for Electrochemical Detection of Ultratrace Explosive Nitroaromatic Compounds. *Electrochem. Commun*. **2007**, *9*, 1719-1724.

32. Tomalia, D. A.; Baker, H.; Dewald, J.; Hall, D. M.; Kallos, G.; Martin , S.; Roeck, J.; Ryder, J.; Smith. A New Class of Polymers; Starburst-Dendritic Macromolecules. *Polymer J.* **1982,** *17,* 117-132.

33. Zeng, F.; Zimmerman, S. C. Dendrimers in Supramolecular Chemistry: From Molecular Recognition to Self-Aassembly. *Chem. Rev*. **1997,** *97,* 1681-1712.

34. Newkome, G. R.; He, E.; Moorefield, C. N. Suprasupermolecules with Novel Properties: Metallodendrimers. *Chem. Rev.* **1999,** *99,* 1689-1746.

35. Smith, D. K.; Diederich, F. Supramolecular Dendrimer Chemistry: A Journey Through the Branched Architecture. *Top. Curr. Chem.* **2000,** *210,* 183-227.

36. Emrick, T.; Fréchet, J. M. J. Self-assembly of Dendritic Structures. *Curr. Opin. Colloid Interf. Sci.* **1999,** *4,* 15-23.

37. Bosman, A. W.; Janssen, H. M.; Meijer, E. W. About Dendrimers: Structure, Physical Properties, and Applications. *Chem. Rev.* **1999,** *99,* 1665-1688.

38. Zhang, W.; Simanek, E. E. Dendrimers Based on Melamine. Divergent and Orthogonal, Convergent Syntheses of a G3 Dendrimer. *J. Am. Chem. Soc.* **2000,** *2,* 843-845.

39. Han, H. J.; Kannan, R. M.; Wang, S.; Mao, G.; Kusanovic J. P.; Romero. Multifunctional Dendrimer-Templated Antibody Presentation on Bionsensor Surfaces for Improved Biomarker Detection. *Adv. Funct. Mater.* **2010,** *20,* 409-421.

40. Yoon, H. C.; Hong, M. Y.; Kim, H. S. Affinity Biosensor for Avidin Using a Double Functionalized Dendrimer monolayer on a Gold Electrode. *Analy. Biochem.* **2000,** *282,* 121-128.

41. Valerio, C.; Fillaut, J. L.; Ruiz, J.; Guittard, J.; Blais, J. C.; Astruc, D. The Dendritic Effect in Molecular Recognition: Ferrocene Dendrimers and Their Use as Supramolecular Redox Sensors for the Recognition of Small Inorganic Anions. *J. Am. Chem. Soc.* **1997**, *119*, 2588-2589.

42. Tomalia, D. A.; Naylor, A. M.; Goddard, W. A., III. Starburst Dendrimers: Molecular-level Control of Size, Shape, Surface Chemistry, Topology, and Flexibility from Atoms to Macroscopic Matter. *Angew. Chem. Int. Edit.* **1990**, *29*, 138-175.

43. Ornelas, C.; Ruiz, A. J.; Cloutet, E.; Alves, S.; Astruc, D. Click Assembly of 1,2,3-Triazole-linked Dendrimers, Including Ferrocenyl Dendrimers, Which Sense Both Oxo Anions and Metal Cations. *Angew. Chem. Int. Edit.* **2007**, *46*, 872-877.

44. Goodson, T., III; Varnavski, O.; Wang, Y. Optical Properties and Applications of Dendrimer-metal Nanocomposites. *Int. Rev. Phys. Chem.* **2004**, *23*, 109-150.

45. Wang, W.; Sun, H.; Kaifer, E. A. Redox Active, Hybrid Dendrimers Containing Fréchet- and Newkome-type Blocks. *Org. Lett.* **2007**, *9*, 2657-2660.

46. Ispasoiu, R. G.; Balogh, L.; Varnavski, O. P.; Tomalia, D. A.; Goodson, T. Large Optical Limiting from Novel Metal-dendrimer Nanocomposite Materials. *J. Am. Chem. Soc.* **2000**, *122*, 11005-11006.

47. Samoc, M.; Samoc, A.; Luther-Davies, B.; Humphrey, M. G.; Wong, M. S. Third-order Optical Nonlinearities of Oligomers, Dendrimers and Polymers Derived from Solution *Z*-scan Studies. *Opt. Mater.* **2003**, *21*, 485-488.

48. Astruc, D.; Boisselier, E.; Ornelas, C. Dendrimers Designed for Functions: From Physical, Photophysical, and Supramolecular Properties to Applications in Sensing, Catalysis, Molecular Electronics, Photonics, and Nanomedicine. *Chem. Rev.* **2010**, *110*, 1857-1959.

49. Boas, U.; Christensen, J. B.; Heegaard, P. M. H. *Dendrimers in Medicine and Biotechnology: New Molecular Tools*; RSC Publishing: Cambridge, UK, **2006**.

50. Mintzer, M. A.; Grinstaff, M. W. Biomedical Applications of Dendrimers: A Tutorial. *Chem. Soc. Rev.* **2011**, *40*, 173-190.

51. Röglin, L.; Lempens, E. H. M.; Meijer, E. W. A Synthetic "Tour de Force": Well-defined Multivalent and Multimodal Dendritic Structures for Biomedical Applications. *Angew. Chem. Int. Edit.* **2011**, *50*,102-112.

52. Cameron, D. J. A.; Shaver, M. P. Aliphatic Polyester Polymer Stars: Synthesis, Properties and Applications in Biomedicine and Nanotechnology. *Chem. Soc. Rev.* **2011**, *40*, 1761-1776.

53. Powell, C. E.; Hurst, S. K.; Morrall, J. P.; Cifuentes, M. P.; Roberts, R. L.; Samoc, M.; Humphrey, M. G. Organometallic Complexes for Nonlinear Optics. 39. Syntheses and Third-order Nonlinear Optical Properties of First-generation

Peripherally Metalated Arylalkynyl Dendrimers. *Organometallics* **2007**, *26*, 4456-5576.

54. Majoral, J. P. State of the Art Developments in the Chemistry and Properties of Dendrimers and Hyperbranched Polymers. *New J. Chem.* **2007**, *31*, 1039-1040.
55. Al-Jamal, K. T.; Ramaswamy, C.; Florence, A. T. Supramolecular Structures from Dendrons and Dendrimers. *Adv. Drug Deliv. Rev.* **2005**, *57*, 2238-2270.
56. Cifuentes, M. P.; Powell, C. E.; Morrall, J. Electrochemical, Spectroelectrochemical, and Molecular Quadratic and Cubic Nonlinear Optical Properties of Alkynylruthenium Dendrimers. *J. Am. Chem. Soc.* **2006**, *128*, 10819-10832.
57. Kraft, A.; Grimsdale, A. C.; Holmes, A. B. Electroluminescent Conjugated Polymers-Seeing Polymers in a New Light. *Angew. Chem. Int. Edit.* **1998**, *37*, 402-428.
58. Lo, S. C.; Burn, P. L. Development of Dendrimers: Macromolecules for Use in Organic Light-emitting Diodes and Solar Cells. *Chem. Rev.* **2007**, *107*, 1097-1116.
59. Morales-Espinoza, E. G.; Lijanova, I. V.; Morales-Saavedra, O. G.; Torres-Zuñiga, V.; Hernandez-Ortega, S.; Martínez-García, M. Synthesis of Porphyrin-Dendrimers with a Pyrene in the Periphery and Their Cubic Nonlinear Optical Properties. *Molecules*, **2011**, *16*, 6950-6968.

60. Hodge, P. Polymer Science Branches Out. *Nature.* **1993,** *362,* 18-19.

61. Klajnert, B.; Bryszewska, M. Dendrimers: Properties and Applications. *Acta Biochimica Polanica.* **2001,** *48,* 199-208.

62. Czerniewski, A. A.; Liu, X. J.; Rollan, O.; Hourani, R.; Four, M.; Kakkar, A.; Templating Silica Network Construction Using 3,5-Dihydroxybenzylalcohol based Dendrimers: Influence of Dendrimer Aggregation on Evolving Network Structure. *J. Mater. Chem.* **2007,** *17,* 2737-2745.

63. Yoo, S.; Lunn, J. D.; Gonzalez, S.; Ristich, J. A.; Simanek, E. E.; Shantz, D. F. Engineering Nanospaces: OMS/Dendrimer Hybrids Possessing Controllable Chemistry and Porosity. *Chem. Mater.* **2006,** *18,* 2935-2942.

64. Jansen, J. F. G. A.; Brabender-van den Berg, E. M. M.; Meijer, E. W. Encapsulation of Guest Molecules into a Dendritic Box. *Science.* **1997,** *266,* 1226-1229.

65. Wells, M.; Crooks, R.M. Interactions between Organized, Surface-Confined Monolayers and Vapor-Phase Probe Molecules. 10. Preparations and Properties of Chemically Sensitive Dendrimer Surfaces. *J. Am. Chem. Soc.* **1996,** *118,* 3988-3989.

66. Bhagiyalakshimia, M.; Park, S. D.; Cha, W.S. Jang, H. T. Development of TREN Dendrimers over Mesoporous SBA-15 for CO_2 Adsorption. *Appl. Surf. Sci.* **2010,** *256,* 6660-6666.

67. Zhijian, L.; Bandar, F.; Schneider, C. J.; Chaffee, A. L. Stepwise Growth of Melamine-based Dendrimers into Mesopores and Their CO_2-Adsoption Properties. *Micropor. Mesopor. Mater.* **2008**, *122*, 536-543.

68. Bandar, F.; Milton, A.; Chaffee, A. L. CO_2 Adsorption by PAMAM Dendrimers: Significant Effect of Impregnation into SBA-15. *Micropor. Mesopor. Mater.* **2009,** *123,* 140-149.

69. Shinn, M.; Robertson, W. M. Surface Plasmon-Like Sensor Based on Surface Electromagnetic Waves in a Photonic Band-Gap Material. *Sensors Actuators B.* **2005,** *105,* 360-364.

70. Farmer, A. F.; Friedli, A. C.; Wright, S. M.; Robertson, W. M. Biosensing Using Surface Electromagnetic Waves in Photonic Band Gap Multilayers. *Sensors Actuators B*. **2012,** *173*, 79-84.

71. Friedli, A. C.; Wright, S. M.; Robertson, W. M. Biosensor Research: SERRI Phase I and II Final Reports, Oak Ridge National Laboratory. August **2010,** December **2011**. http://www.serri.org/publications/Pages/Reports.aspx. Accessed June, 2013

72. Peter Haddix, Unpublished Results.

73. Hsiao, V. K.; Waldeisen, J. R.; Zheng, Y.; Lloyd, P. F; Bunning, T. J.; Huang, T. J. Aminopropyltriethoxysilane (APTES)-functionalized Nanoporous Polymeric

Gratings: Fabrication and Application in Biosensing. *J. Mater. Chem.* **2007**, *17*, 4896-4901.

74. Adam F. Farmer, Honors Thesis, 2004, "Development of a Biosensor"
75. Zeng, X.; Xu, G.; Gao, Y.; An, Y. Surface Wetting of (3-Aminopropyl)-triethoxy-silane Self-Assembled Monolayers. *J. Phys. Chem*. B, **2011**, *115*, 450-454.
76. Simanek, E. E.; Abdou, H.; Lalwani, S.; Lim, J.; Mintzer, M.; Venditto, V. J.; Vittur, B. The 8 Year Thicket of Triazine Dendrimers: Strategies, Targets and Applications. *Proc. R. Soc. A.* **2010**, *466*, 1445-1468
77. Cole, K. D.; Cothron, P. J.; Davis, C. L.; Standley, T. A; Friedli, A. C. "Nanoimprinted Organosilicates for Detection of Aromatic and Nitroaromatic Compounds." 237th National Meeting of the American Chemical Society, March 22-26, 2009, Salt Lake City, UT. Abstract CHED 247. (Poster)